Paramagnetic NMR Investigations of High-Spin Nickel(II) Complexes. Controlled Synthesis, Structural, Electronic, and Magnetic Properties of Dinuclear vs Mononuclear Species

Catherine Belle,*,† Catherine Bougault,*,† Marie-Thérèse Averbuch,† André Durif,† Jean-Louis Pierre,† Jean-Marc Latour,‡ and Laurent Le Pape‡

Contribution from the Laboratoire d'Etudes Dynamiques et Structurales de la Sélectivité (LEDSS, UMR CNRS 5616), Université Joseph Fourier, BP 53X, 38041 Grenoble Cedex 9, France, and the Service de Chimie Inorganique et Biologique (SCIB, UMR CNRS 5046), DRFMC/CEA-Grenoble, 17 rue des Martyrs, 38054 Grenoble Cedex 9, France

Received February 7, 2001. Revised Manuscript Received May 1, 2001

Abstract: New dissymmetric tertiary amines (N_3SR) with varying N/S donor sets have been synthesized to provide mono- and dinuclear complexes. Acetate ions are used to complete the octahedral coordination sphere around nickel(II) atom(s). The facile conversion of mononuclear to dinuclear systems can be controlled to produce either mono- or dinuclear complexes from the same ligand. The dinuclear complex **a(BPh$_4$)$_2$** ([$Ni_2(N_3SSN_3)(OAc)_2$](BPh_4)$_2$) has been characterized in the solid state by X-ray diffraction techniques as solvate: **a(BPh$_4$)$_2$**·$^1/_2$[5(CH_3OH)·(CH_3CN)·(CH_3CH_2OH)]. The two Ni atoms are six-coordinated and bridged by a disulfide group and two bidentate acetates. Magnetic susceptibility reveals a weak ferromagnetic exchange interaction between the two Ni atoms with $J = 2.5(7)$ cm^{-1}. UV−vis studies suggest that the six-coordinated structure persists in solution. The ^{1}H NMR spectrum of **a(BPh$_4$)$_2$** exhibits sharp significantly hyperfine shifted ligand signals. A complete assignment of resonances is accomplished by a combination of methods: 2D-COSY experiments, selective chemical substitution, and analysis of proton relaxation data. Proton isotropic hyperfine shifts are shown to originate mainly from contact interactions and to intrinsically contain a small *J*-magnetic coupling and/or zero-field splitting contribution. A temperature dependence study of longitudinal relaxation times indicates that a very unusual paramagnetic Curie dipolar mechanism is the dominant relaxation pathway in these weakly ferromagnetically spin-coupled dinickel(II) centers. The mononuclear nickel(II) analogue exhibits extremely broader ^{1}H NMR signals and only partial analysis could be performed. These data are consistent with a shortening of electronic relaxation times in homodinuclear compounds with respect to the corresponding mononuclear species.

Introduction

Growing interest, in the past decade, has been directed toward nickel as a biologically and spectroscopically relevant metal. To date, natural occurrence of nickel(II) has been evidenced in six types of enzymes: ureases, where it catalyzes the hydrolysis of urea, and hydrogenases, methyl coenzyme M reductase, carbon monoxide dehydrogenase, acetyl coenzyme A synthase, and nickel superoxide dismutase, where it is known to present redox activity.[1] A detailed picture of the active site of two of these enzymes, [Ni−Fe] hydrogenase[2,3] and urease,[4−7] has emerged through recent X-ray crystallographic studies. In addition to elucidation of the coordination structure at the metal center, it is of fundamental interest to understand the mechanisms, which control substrate conversion or inhibition pathways of these enzymes. In that respect, NMR techniques can provide a wealth of unique information on the electronic, magnetic, and molecular properties of the metal-binding sites, and thus allow extraction of crucial mechanistic data.[8,9]

Contact and dipolar interactions between the considered nucleus and the metal induce hyperfine shifts of NMR signals and shortening of nuclear relaxation times. High-resolution NMR can nevertheless be successfully performed and data can be interpreted in cases where electronic relaxation times of the metal are short enough, usually 10^{-11}−10^{-12} s, as in low-spin

* To whom correspondence should be addressed. E-mail: *Catherine.Belle@ujf-grenoble.fr. Catherine.Bougault@ujf-grenoble.fr.* FAX: (33) 4 76 51 48 36.

† LEDSS: Laboratoire d'Etudes Dynamiques et Structurales de la Sélectivité.

‡ SCIB: Service de Chimie Inorganique et Biologique.

(1) For recent reviews, see: (a) Cammack, R.; van Vliet, P. In *Bioinorganic Catalysis*; Reedjik, J., Bouwman, E., Eds.; Marcel Dekker: New York, 1999; pp 231−268. (b) Ermler, U.; Grabarse, W.; Shima, S.; Goubeaud, M.; Thauer, R. K. *Curr. Opin. Struct. Biol.* **1998**, *8*, 749−758. (c) Maroney, M. J.; Davidson, G.; Allan, C. B.; Figlar, J. *Struct. Bonding* **1998**, *92*, 1−65. (d) Ragsdale, S. W. *Curr. Opin Chem. Biol.* **1998**, *2*, 208−215.

(2) Volbeda, A.; Garcin, E.; Piras, C.; de Lacey, A. L.; Fernandez, V. M.; Hatchikian, E. C.; Frey, M.; Fontecilla-Camps, J. C. *J. Am. Chem. Soc.* **1996**, *118*, 12989−12996.

(3) Davidson, G.; Choudhury, S. B.; Gu, Z. J.; Bose, K.; Roseboom, W.; Albracht, S. P. J.; Maroney, M. J. *Biochemistry* **2000**, *39*, 7468−7479 and references therein.

(4) Jabri, E.; Carr, M. B.; Hausinger, R. P.; Karplus, P. A. *Science* **1995**, *268*, 998−1004.

(5) Pearson, M. A.; Michel, L. O.; Hausinger, R. P.; Karplus, P. A. *Biochemistry* **1997**, *36*, 8164−8172.

(6) Benini, S.; Rypnievski, W. R.; Wilson, K. S.; Miletti, S.; Ciurli, S.; Mangani, S. *Structure* **1999**, *7*, 205−216.

(7) Benini, S.; Rypniewski, W. R.; Wilson, K. S.; Ciurli, S.; Mangani, S. *J. Biol. Inorg. Chem.* **1998**, *3*, 268−273.

(8) Bertini, I.; Turano, P.; Vial, A. *Chem. Rev.* **1993**, *93*, 2833−2932.

(9) See: *Biological Magnetic Resonance, NMR of Paramagnetic Molecules Proteins*; Berliner, L. J., Reuben, J., Eds.; Plenum Press: New York, 1993; Vol. 12.

10.1021/ja010342k CCC: $20.00
Published on Web 07/28/2001

Fe^{III} [10] and high-spin Co^{II} samples.[8] Electronic relaxation times for high-spin nickel(II) are typically $10^{-10}-10^{-12}$ s. In the most favorable case (i.e, pseudotetrahedral or high-spin pentacoordinated nickel(II)), reasonably sharp and well-resolved NMR signals are observed and structural information can be retrieved.[11,12] For instance, Ni^{II}-substitution of Zn^{II}, Cu^{II}, and Fe^{II} was advantageously introduced for NMR studies of a variety of metalloproteins.[13−17] In octahedral nickel(II) monomers, electronic relaxation times are usually longer and observed resonances are consequently broader.[18,19] When more than one paramagnetic center is present in the same molecule, the situation may however be completely different. Recent NMR studies on copper(II) homodimers showed in fact that nuclear relaxation enhancement and relatively sharp signals may be observed in dinuclear species, while mononuclear analogues gave rise to broad ^{1}H NMR resonances. Studies on model complexes lead to suspecting the spin-coupling interactions between paramagnetic centers are responsible for the more efficient overall electronic relaxation and the subsequent sharpness of NMR signals.[20,21] The real origin of this behavior is nevertheless far from clear.[22,23] Systematic studies on a large variety of homodimers with an extended range of *J*-values are then necessary. To date, NMR properties of compounds containing octahedral nickel(II) remain largely unexplored and, to our knowledge, no ^{1}H NMR data have been reported on dimeric species, while both ferromagnetic and antiferromagnetic (large and weak) *J*-coupling constants have been reported. Correlation of the structural, magnetic, and ^{1}H NMR features may then provide a fundamental insight into the description and understanding of the relaxation mechanisms in paramagnetic clusters.

In the present study, synthesis of nonsymmetric tertiary amines (N_3SR, Scheme 1) and preparation of mono- and dinuclear octahedral nickel(II) complexes are extensively described. One of the latter, the **a(BPh$_4$)$_2$** complex ($[Ni_2(N_3SSN_3)(OAc)_2](BPh_4)_2$), is fully characterized. Assignment of proton resonances can be completely achieved using 2D NMR methodology and T_1 relaxation measurements with the help of X-ray crystal data and magnetic susceptibility results. The possible implications of the *J* spin-coupling constant and intrinsic zero-field splitting of each nickel(II) on the observed enhanced nuclear relaxation are discussed. The present approach demonstrates that ^{1}H NMR is a viable tool for studying octahedral nickel(II) dimeric species in solution and may be relevant when applied to wild-type or engineered dinuclear nickel metalloproteins.

Scheme 1

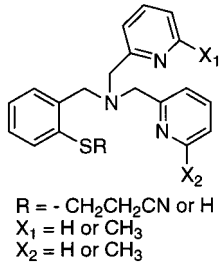

Experimental Section

General Methods. Commercial reagents were used as obtained without further purification. Solvents were purified by standard methods before use. Elemental analyses were performed by the CNRS Microanalysis Laboratory of Lyon, France. Mass spectra were recorded on a Nermag R 1010C apparatus. Fast-atom bombardment (FAB) in the positive mode were obtained with the spectrometer equipped with a M scan (Wallis) atom gun (8 kV, 20 mA). IR (KBr disks) spectra were recorded on a Nicolet 550 FT-IR spectrometer. UV−visible spectra were obtained using a Perkin-Elmer Lambda 2 spectrophotometer operating in the range 200−1100 nm with quartz cells. Extinction coefficients ϵ are given in $M^{-1}\cdot cm^{-1}$. ^{1}H NMR spectra of organic compounds were recorded on a BRUKER AC 200 spectrometer, at 25 °C. Chemical shifts in ppm were referenced to residual solvent peaks.

Syntheses: Ligand Syntheses. Experimental details relative to the syntheses of **6**, **7**, and **9** and to physicochemical properties of compounds **1** to **4** and **6** to **9** (elemental analysis, ^{1}H and ^{13}C NMR, as well as mass spectrometry data) are provided as Supporting Information.

1: Under an inert atmosphere, a solution of thiosalicylic acid (1 g, 6.29 mmol) in 20 mL of dry THF was added to a suspension, in dry THF (5 mL), of NaH (60% in oil, 500 mg, 12.58 mmol), previously washed with dry pentane. The mixture was cooled with an ice bath during the addition. The suspension was stirred subsequently for 1 h at room temperature. A solution of 3-bromopropionitrile in THF (20 mL) was then added dropwise, and the mixture was heated and refluxed for 12 h under vigorous stirring. After the mixture was cooled, the THF was removed in vacuo. The residue was melted in water and 4 N HCl was added to the mixture up to precipitation of a white solid. A small amount of dichloromethane was added to this suspension and the product was isolated by filtration, washed with pentane, and dried under vacuum. **1** was obtained as a white powder (1.24 g, 5.99 mmol) with 95% yield and used in the following steps without further purification. An analytical sample was obtained after recrystallization from dichloromethane/acetone: mp 185 °C.

2: A solution of ethyl chloroformate (0.25 mL, 2.61 mmol) in distilled THF (5 mL) was added at −5 °C to a mixture of acid **1** (0.5 g, 2.40 mmol), NEt_3 (0.3 mL, 2.16 mmol), and distilled THF (15 mL). The mixture was allowed to stir for 1 h at −5 °C. After filtration, the filtrate was treated with an excess of $NaBH_4$ in H_2O (10 mL) at 0 °C. The mixture was allowed to warm to room temperature and was stirred for 12 additional hours. The suspension was further acidified with 4 N HCl to pH 1, and the solvent was removed under reduced pressure. The residue was taken up with water and extracted three times with ethyl acetate. The organic extracts were neutralized with a solution of $NaHCO_3$ and washed with H_2O and brine. The obtained organic layer was dried over Na_2SO_4 and reduced in vacuo to yield the pure product **2** as a pale yellow oil (396 mg, yield 85%) which solidified upon standing at −20 °C.

3: The alcohol **2** was added (1 g, 5.18 mmol) to a suspension of MnO_2 (5.3 g, 51.80 mmol) in dry dichloromethane (50 mL). The

(10) For a review, see: La Mar, G. N.; de Ropp, J. S. *NMR Methodology for Paramagnetic Proteins*; pp 1−78 in ref 9.
(11) Sacconi, L.; Mani, F.; Bencini, A. In *Comprehensive Coordination Chemistry*; Wilkinson, S. R., Gillard, R. D., McCleverty, J. A., Eds.; Pergamon Press: Oxford, 1987; Vol. 5, pp 56−60.
(12) Baidya, N.; Olmstead, M. M.; Whitehead, J. P.; Bagyinka, C.; Maroney, M. J.; Mascharak, P. K. *Inorg. Chem.* **1992**, *31*, 3612−3619.
(13) Moratal Mascarell, J. M.; Martinez Ferrer, M.-J.; Jimenez, H. R.; Donaire, A.; Castells, J.; Salgado, J. *J. Inorg. Biochem.* **1992**, *45*, 231−243.
(14) (a) Donaire, A.; Salgado, J.; Moratal, J.-M. *Biochemistry* **1998**, *37*, 8659−8673. (b) Salgado, J.; Kalverda, A. P.; Diederix, R. E. M.; Canters, G. W.; Moratal, J. M.; Lawler, A. T.; Dennison, C. *J. Biol. Inorg. Chem* **1999**, *4*, 457−467.
(15) Fernandez, C. O.; Sannazzaro, A. I.; Diaz, L. E.; Vila, A. J. *Inorg. Chim. Acta* **1998**, *273*, 367−371.
(16) Moura, I.; Teixeira, M.; LeGall, J.; Moura, J. J. G. *J. Inorg. Biochem.* **1991**, *44*, 127−139.
(17) Luchinat, C.; Ciurli, S. *NMR of Polymetallic Systems in Proteins*; pp 357−420 in ref 9.
(18) Rosenfield, S. G.; Berends, H. P.; Gelmini, L.; Stephan, D. W.; Mascharak, P. K. *Inorg. Chem.* **1987**, *26*, 2792−2797.
(19) Dietz, C.; Heinemann, F. W.; Kuhnigk, J.; Krüger, C.; Gerdan, M.; Trautwein, A. X.; Grohmann, A. *Eur. J. Inorg. Chem.* **1998**, 1041−1049.
(20) Brink, J. M.; Rose, R. A.; Holz, R. C. *Inorg. Chem.* **1996**, *35*, 2878−2885.
(21) Asokan, A.; Varghese, B.; Manoharan, P. T. *Inorg. Chem.* **1999**, *38*, 4393−4399.
(22) Murthy, N. N.; Karlin, K. D.; Bertini, I.; Luchinat, C. *J. Am. Chem. Soc.* **1997**, *119*, 2156−2162.
(23) Holz, R. C.; Bennett, B.; Chen, G.; Ming, L.-J. *J. Am. Chem. Soc.* **1998**, *120*, 6329−6335.

mixture was heated and refluxed for 2 h. After cooling, filtration over Celite, and evaporation in vacuo, the crude product was isolated as a yellow solid. Recrystallization in diethyl ether/hexane afforded 0.95 g (97%) of white solid **3**: mp 64 °C.

4: A 2.00 g sample of **3** (10 mmol) was dissolved in 125 mL of MeOH and 0.91 mL of 2-(aminomethyl)pyridine (8.73 mmol) was added to the reaction vessel. The solution was refluxed and stirred for 2 h. After the mixture was cooled, the resulting Schiff's base was reduced with $NaBH_4$ (0.85 g, 21 mmol) and the mixture was stirred for 12 h. Then, 4 N HCl was added to the ice-cold suspension and the solvent was removed under reduced pressure. The residue was taken up with water and extracted with dichloromethane. Then the aqueous extract was neutralized with a $NaHCO_3$ solution and extracted three times with portions of dichloromethane. The combined organic extracts were dried over sodium sulfate. The solvent was removed under reduced pressure affording the yellow oil **4** (2.4 g, 8.54 mmol, 98% yield). The product was used without any purification. Compound **8** was prepared with 51% overall yield, according to this procedure. Compound **7** was obtained from 2-formaldoxime-6-methylpyridine, using modifications of a previously reported procedure.[24]

5: A solution of **4** (1.08 g, 3.83 mmol) in dry methanol (50 mL) containing 1.1 mL of glacial acetic acid was added to a solution of pyridine-2-carboxaldehyde (442 μL, 4.6 mmol) in 50 mL of dry methanol. $NaBH_3CN$ (1 g, 15.32 mmol) was added to the reaction mixture under a nitrogen atmosphere, and the suspension was stirred for 3 days. After this period, the pH of the ice-cold reaction mixture was adjusted to 2.0 by careful addition of concentrated HCl, and the mixture was stirred for an additional hour. The solution was reduced to dryness under reduced pressure, and the resulting residue was redissolved in 30 mL of water. The aqueous solution was washed two times with dichloromethane, and the pH of the solution was then adjusted to about 8 by addition of $NaHCO_3$. The resulting slightly basic solution was then extracted four times with dichloromethane. The extracts were combined, washed with brine, and dried over anhydrous Na_2SO_4. The solvent was removed in vacuo to give 1.23 g of crude product as a brown oil. The later was purified by chromatography on neutral alumina and eluted with ethyl acetate/cyclohexane (2:1,v /v) to give 1.07 g (75% yield) of oil **5** (2.87 mmol). ^{1}H NMR ($CDCl_3$) δ 8.51 (d, 2H, J = 4.1 Hz, Py-*H1*), 7.60 (m, 4H, Ar-*H*), 7.2 (m, 6H, Ar-*H*), 3.98 (s, 2H, NCH_2ArSR), 3.94 (s, 4H, NCH_2Py), 3.06 (t, 2H, J = 7.2 Hz, −SCH_2−), 2.54 (t, 2H, J = 7.2 Hz, −CH_2CN); ^{13}C NMR ($CDCl_3$) δ 159.3, 148.7, 137.7, 136.1, 132.4, 131.2, 129.6, 127.7, 126.7, 122.0, 121.6, 117.8, 54.3, 51.3, 29.7, 17.8; mass spectrum (EI), *m*/*z* 375 $[M]^+$. Anal. Calcd for $C_{22}H_{22}N_4S$: C, 70.56; H, 5.92; N, 14.96; S, 8.56. Found: C, 70.66; H, 5.94; N, 14.91; S, 8.58. Compounds **6** and **9** were prepared according to this procedure.

Preparation of Dinuclear Complex a(BPh$_4$)$_2$. Syntheses (according to method A) and physicochemical properties (elemental analysis, UV−vis, IR, as well as mass spectrometry data) of PF_6 salts of the dinuclear complexes, **a(PF$_6$)$_2$**, **b(PF$_6$)$_2$**, and **c(PF$_6$)$_2$**, are provided as Supporting Information.

Method A. To a solution of **5** (110 mg, 0.28 mmol) in methanol (2 mL) was added a solution of $Ni(OAc)_2\cdot 4H_2O$ (93 mg, 0.37 mmol) in methanol (7 mL). The blue solution was stirred at room temperature and progressively turned green over 1 day. After an additional day, a solution of $NaBPh_4$ (116 mg, 0.34 mmol) in methanol (3 mL) was added to precipitate the crude product as a powder. Filtration and recrystallization by vapor diffusion of ethanol into an acetonitrile solution of this solid afforded pale-green crystals of X-ray quality. This crystalline material was dried in vacuo and afforded **a(BPh$_4$)$_2$** (68.7 mg, yield 32%). Anal. Calcd for $C_{90}H_{82}N_6O_4S_2Ni_2B_2$: C, 71.27; H, 5.58; N, 5.54; S, 4.23; Ni, 7.74; B, 1.43. Found: C, 71.13; H, 5.41; N, 5.46; S, 4.02; Ni, 7.65; B, 1.42. Mass spectrum (FAB, matrix NBA), *m*/*z* 1195 $[M - BPh_4]^+$; IR (KBr, cm^{-1}) 3042, 2968, 1605, 1580 (ν_{as}(COO)), 1472, 1423 (ν_s(COO)), 703; UV−vis (acetone, λ_{max}, nm (ϵ, $M^{-1}\cdot cm^{-1}$)) 400 (sh), 575 (35), 966 (46).

Method B. A solution of potassium *tert*-butoxide (200 mg, 1.69 mmol) in distilled THF (30 mL) was added slowly (1 h) to a stirred solution of **5** (300 mg, 0.80 mmol) in distilled THF (30 mL) under argon. The mixture was stirred for 2 h and acidified with 4 N HCl. The resulting solution was evaporated in vacuo, and ethanol (30 mL) was added to the residue. After 12 h at 0 °C, the suspension was filtered. The orange filtrate was evaporated in vacuo to provide the solid trihydrochloride salt of the deprotected thiolate from **5** (310 mg). The corresponding free base was recovered by neutralizing the crude product to pH 6 with $NaHCO_3$ in aqueous solution, followed by extraction with CH_2Cl_2. The organic extracts were combined and dried over anhydrous Na_2SO_4. Solvent removal in vacuo afforded 200 mg of yellow oil **10**.[25] ^{1}H NMR ($CDCl_3$) δ 8.49 (d, 2H, J = 4.2 Hz, Py-*H1*), 7.60 (m, 5H, Ar-*H*), 7.35 (m, 1H, Ar-*H*), 7.13 (m, 4H, Ar-*H*), 3.86 (s, 2H, NCH_2-ArSH), 3.80 (s, 4H, NCH_2Py), 1.26 (s br, −S*H*); ^{13}C NMR ($CDCl_3$) δ 158.9, 148.7, 148.4, 137.7, 137.6, 129.9, 128.0, 127.7, 126.3, 123.5, 122.0, 59.5, 56.7; mass spectrum (CI, NH_3), *m*/*z* 322 $[M + H]^+$. To an argon-purged solution of **10** (50 mg, 0.156 mmol) in methanol (3 mL) was added $Ni(OAc)_2\cdot 4H_2O$ (40 mg, 0.158 mmol) in methanol (3 mL). The green solution was stirred for 1 h and a solution of $NaBPh_4$ (106 mg, 0.310 mmol) in methanol (6 mL) was added to induce precipitation of the product as a powder. Filtration and recrystallization by vapor diffusion of ethanol into an acetonitrile solution of this solid afforded crystalline material, which was filtered and dried in vacuo. **a(BPh$_4$)$_2$** (65.7 mg) was isolated with 43% overall yield. This compound was shown to be identical (UV−vis, IR, ^{1}H NMR, mass spectra) to **a(BPh$_4$)$_2$** obtained in method A.

Preparation of Mononuclear Complex m(BPh$_4$). The PF_6 salt of this complex was prepared according to an essentially similar procedure (see Supporting Information for details).

m(BPh$_4$). To a degassed solution of cyanoethyl-protected thiolate **5** (105 mg, 0.28 mmol) in methanol (5 mL) was added $Ni(OAc)_2\cdot 4H_2O$ (70 mg, 0.28 mmol) in methanol (7 mL). After the mixture was stirred for 1 h in argon atmosphere, a solution of $NaBPh_4$ (96 mg, 0.28 mmol) in degassed methanol (5 mL) was added. A gray precipitate formed instantly. The suspension was cooled at −20 °C for 12 h and the precipitate was removed by filtration. The filtrate was concentrated and cooled to −20 °C and after 1 week a violet powder was recovered by filtration, which after drying in vacuo afforded 119 mg (52% yield) of **m(BPh$_4$)**. This material was stable both in the solid state at room temperature and in acetone solution at −20 °C for months. Anal. Calcd for $C_{48}H_{44}N_4O_2SNiB$: C, 71.13; H, 5.47; N, 6.91; S, 3.96; Ni, 7.24; B, 1.33. Found: C, 70.20; H, 5.53; N, 6.90; S, 3.97; Ni, 6.53; B, 1.30. Mass spectrum (FAB, matrix NBA), *m*/*z* 491 $[M - BPh_4]^+$; IR (KBr, cm^{-1}) 3047.5, 2975, 1735, 2252, 1607, 1540 (ν_{as}(COO)), 1487.5, 1426 (ν_s(COO)), 1240, 735; UV−vis (acetone, λ_{max}, nm (ϵ, $M^{-1}\cdot cm^{-1}$)) 334 (148), 550 (10), 941 (16).

Magnetization Data. Magnetization experiments have been performed on a Quantum Design MPMS superconducting quantum interference device (SQUID) magnetometer operating at four magnetic fields, 0.5, 1, 2.5, and 5 T, over the temperature range 4−300 K. The powdered sample **a(BPh$_4$)$_2$** (11.7 mg, 7.72 μmol) was contained in a kel F bucket, whose contribution to the magnetic susceptibility was evaluated independently and subtracted from the sample data. The molar susceptibility corresponds to the resulting magnetization per magnetic field unit per mole. The diamagnetic contributions were estimated from Pascal's constants at -905×10^{-6} $cm^3\cdot mol^{-1}$.

X-ray Data Collection and Crystal Structure Determination. Crystal data, together with details of diffraction experiment and refinement, are summarized in Table 1S (Supporting Information). Single crystals of complex **a(BPh$_4$)$_2$** were obtained as $[Ni_2S_2N_6C_{42}O_4H_{42}]\cdot 2(C_{24}BH_{20})\cdot {}^1/_2$solvate, where solvate = $[5(CH_3OH)\cdot(CH_3CN)\cdot(CH_3CH_2OH)]$ and M_w = 1638.48. A yellowish triclinic prism ($0.22 \times 0.21 \times 0.19$ mm^3) was mounted on a Enraf-Nonius CAD4 diffractometer operating at 293 K with Mo Kα radiation (λ = 0.7107 Å) monochromated by a graphite plate. The compound is triclinic, $P\bar{1}$, with a = 18.128(7) Å, b = 20.224(7) Å, c = 26.221(9) Å, α = 101.30-(2)°, β = 104.07(2)°, γ = 102.37(3)°, V = 8791(6) Å^3, Z = 4, D_x = 1.238 g·cm^{-3}, and μ = 0.533 mm^{-1}. 17557 reflections were collected in the range $4.2° \le 2\theta \le 44.2°$ leading to a set of 16972 independent reflections. The diffraction data were corrected for Lorentz and

(24) Fuentes, O.; Paudler, W. W. *J. Org. Chem.* **1975**, *40*, 1210−1213.

(25) An alternate synthesis of **10** was reported (Burth, R.; Stange, A.; Schäfer, M.; Vahrenkamp, H. *Eur. J. Inorg. Chem.* **1998**, 1759−1764).

Table 1. Main Interatomic Distances (Å) and Bond Angles (deg) in the Two Dicationic $[Ni_2(C_{42}H_{42}N_6O_4S_2)]^{2+}$ Entities $\mathbf{a_1}$ and $\mathbf{a_2}$ from Complex $\mathbf{a(BPh_4)_2}$

first entity ($\mathbf{a_1}$)		second entity ($\mathbf{a_2}$)	
Ni1−Ni2	4.243(1)	Ni3−Ni4	4.299(2)
Ni1−S1	2.527(2)	Ni3−S3	2.517(2)
Ni1−O1	2.067(4)	Ni3−O5	2.042(4)
Ni1−O2	1.981(4)	Ni3−O6	2.006(3)
Ni1−N1	2.088(4	Ni3−N7	2.100(4)
Ni1−N2	2.056(4)	Ni3−N8	2.028(5)
Ni1−N3	2.054(5)	Ni3−N9	2.043(5)
S1−S2	2.073(2)	S4−S3	2.080(2)
Ni2−S2	2.524(2)	Ni4−S4	2.513(2)
Ni2−O3	2.050(4)	Ni4−O7	2.055(4)
Ni2−O4	2.010(3)	Ni4−O8	1.986(4)
Ni2−N4	2.098(4)	Ni4−N10	2.091(4)
Ni2−N5	2.051(5)	Ni4−N11	2.039(5)
Ni2−N6	2.051(5)	Ni4−N12	2.074(5)
S1−Ni1−O1	87.2(1)	S3−Ni3−O5	85.6(1)
S1−Ni1−O2	93.7(1)	S3−Ni3−O6	94.3(1)
S1−Ni1−N1	93.8(1)	S3−Ni3−N7	94.1(1)
N1−Ni1−N3	82.0(2)	S3−Ni3−N8	84.7(1)
S1−Ni1−N3	84.0(1)	S3−Ni3−N9	173.1(1)
O1−Ni1−O2	95.2(2)	O5−Ni3−O6	95.9(2)
O1−Ni1−N1	90.0(2)	O5−Ni3−N7	89.7(2)
O1−Ni1−N2	88.2(2)	O5−Ni3−N8	166.8(2)
N2−Ni1−N3	99.7(2)	O5−Ni3−N9	90.7(2)
N1−Ni1−N2	81.4(2)	O6−Ni3−N7	170.3(2)
O2−Ni1−N2	91.5(2)	O6−Ni3−N9	91.9(2)
O2−Ni1−N3	94.0(2)	N7−Ni3−N8	82.1(2)
S1−Ni1−N2	173.4(1)	N7−Ni3−N9	80.0(2)
O1−Ni1−N3	167.7(2)	N8−Ni3−N9	97.9(2)
O2−Ni1−N1	171.1(2)	O6−Ni3−N8	93.8(2)
O4−Ni2−N6	91.7(2)	O7−Ni4−N11	89.3(2)
N4−Ni2−N5	82.1(2)	O7−Ni4−N12	166.2(2)
N4−Ni2−N6	79.8(2)	O8−Ni4−N10	170.5(2)
N5−Ni2−N6	98.9(2)	O8−Ni4−N11	91.7(2)
S2−Ni2−O3	87.6(1)	O8−Ni4−N12	95.2(2)
S2−Ni2−O4	95.0(1)	N10−Ni4−N11	80.0(2)
S2−Ni2−N4	94.0(1)	N10−Ni4−N12	81.7(2)
S2−Ni2−N5	85.3(1)	N11−Ni4−N12	99.6(2)
O4−Ni2−N5	93.3(2)	S4−Ni4−N12	83.5(1)
O3−Ni2−N6	87.2(2)	O7−Ni4−O8	94.9(2)
O3−Ni2−N4	89.2(2)	S4−Ni4−N10	94.5(1)
O3−Ni2−O4	96.4(1)	O7−Ni4−N10	89.7(2)
O4−Ni2−N4	169.5(2)	S4−Ni4−O7	86.6(1)
S2−Ni2−N6	172.0(1)	S4−Ni4−O8	94.1(1)
O3−Ni2−N5	168.3(2)	S4−Ni4−N11	173.2(2)

polarization effects, but not for absorption. Crystal structure was solved by direct methods[26a] using the texsan software.[26b] All non-hydrogen atoms were refined with anisotropic thermal parameters. Almost all hydrogen atoms were located by difference Fourier syntheses, but not refined. All the components of the solvate have high thermal motions. Owing to the great number of parameters to be refined, the solvate components were only refined in the early steps of the crystal structure determination and then fixed. Final cycle refinement, including 1909 parameters, converged to $R(F) = 0.059$ and $Rw(F) = 0.060$ for 11586 $F > 1\sigma(F)$, $S = 1.973$, $\Delta/\sigma_{max} = 0.01$, $\Delta\rho_{max} = 0.44$ e·Å^{-3}, and $\Delta\rho_{min} = -0.41$ e·Å^{-3}. Structure overlays and comparisons, identification of pseudosymmetry axes, interatomic distances, as well as dihedral angles were obtained from Insight II software,[26c] where the crystallographic .pdb file could be easily retrieved.

NMR Data. A Varian Unity 400 spectrometer, equipped with an extended-duration liquids Variable Temperature Control unit and a 50-L dewar filled with liquid nitrogen, was used for collection of both 1D and 2D NMR spectra at the required temperature. A temperature calibration curve was recorded on the temperature range 188−378 K using methanol (188−283 K) and ethylene glycol (283−378 K). The spectral window for ^{1}H NMR data acquisition was adjusted for each collected temperature. A typical spectrum consisted of 16K data points, 512 scans on the whole spectral bandwidth, and a 500 ms relaxation delay. An exponential weighting function (lb = 10 Hz) was used during processing. Enhancement of the resolution in the [−20 ppm, 100 ppm] spectral region was achieved using 32K data points, 512 scans, and a 1−5 Hz line broadening exponential function on the corresponding 48 kHz bandwidth. Chemical shifts (in ppm) were referenced to the residual solvent peak at 2.04 and 5.32 ppm for CD_3COCD_3 and CD_2Cl_2, respectively. Inversion−recovery pulse sequence [180°−τ−90°−AQ] was set up with 36 variable delay values ranging from 10 μs to 200 ms. The 90° pulse (7.3 μs) was calibrated at 293 K and dictated a maximum 34 kHz spectral bandwidth for nonselective T_1 measurements. Acquisition windows were consequently adjusted to avoid peak folding in the spectral region of interest. Relaxation time calculations involved a monoexponential fitting procedure of the intensities vs τ values for each selected resonance. A typical magnitude COSY spectrum was collected with 512 t_1 blocks of 4096 t_2 data points and 2048 scans over a 32 kHz bandwidth with a recycle time of 163 ms. Zerofilling to 1024 data points was performed in the t_1 dimension prior to Fourier transformation and experimental data were processed using unshifted sinebell apodization functions in both dimensions. Standard least-squares fit procedures were used to process data showing the temperature dependence of observed chemical shifts or relaxation rates.

Results and Discussion

Ligands Preparations. A series of nonsymmetric tertiary amines N_3SR (Scheme 1) are synthesized from thiosalicylic acid and first require protection of the thiolate function to avoid oxidation (Figure 1). The cyanoethyl-protecting group is used here: it is more easily introduced and removed than the largely used *tert*-butyl group and has the virtue of easier workup conditions and higher yields.[27−29] On the other hand, it is known that metal ions such as copper(II)[30] or nickel(II)[31,32] may cleave the S-*tert*-butyl linkage present in a multidonor protected ligand by refluxing the protected ligand with metallic salts in alcohol solution. This approach with the cyanoethyl group is then applied here.

The cyanoethyl-protected thiolate compound **1** is prepared by alkylation with 3-bromopropionitrile in refluxing THF (95% yield). Then, reaction with ethyl chloroformate and NEt_3 followed by reduction with $NaBH_4$[33] gives the alcohol **2** in 85% yield. Conversion of **2** to the desired aldehyde **3** is accomplished by oxidation with MnO_2 in dichloromethane (97% yield). Upon addition of the 2-(aminomethyl)pyridine or primary amine **7** to the aldehyde **3**, and reduction, the corresponding nonsymmetric amines **4** and **8** are obtained via the procedure outlined in Figure 1. The iminium ion resulting from the condensation of the secondary amine **4** with pyridine-2-carboxaldehyde or 6-methylpyridine-2-carboxaldehyde (or from the condensation of amine **8** with 6-methylpyridine-2-carboxaldehyde) is reduced using $NaBH_3CN$.[34] The desired ligands **5** (75% yield), **6** (67% yield),

(26) (a) Altomare, A.; Cascarano, A.; Giacovazzo, G.; Guagliardi, A. *J. Appl. Crystallogr*. **1993**, *26*, 343−350. (b) *TEXAN, Single-Crystal Structure Analysis Software*, Version 1.7; Molecular Structure Corporation: The Woodlands, TX, 1995. (c) *Insight II Software*, Version 98.0, run on a IBM Risc Graphic Station; Molecular Simulations Inc.: San Diego, 1998.

(27) Nikiforov, T. T.; Connolly, B. A. *Tetrahedron Lett.* **1992**, *33*, 2379−2382.

(28) Dahl, B. H.; Bjergårde, K.; Sommer, V. B.; Dahl, O. *Acta Chem. Scand.* **1989**, *43*, 896−901.

(29) Svenstrup, N.; Rasmussen, K. M.; Hansen, T. K.; Becher, J. *Synthesis* **1994**, 809−812.

(30) Becher, J.; Toftund, H.; Olesen, P. H. *J. Chem. Soc., Chem. Commun*. **1983**, 740−742.

(31) Dutton, J. C.; Fallon, G. D.; Murray, K. S. *Chem. Lett.* **1990**, 983−986.

(32) Bouwman, E.; Henderson, R. K.; Powell, A. K.; Reedijk, J.; Smeets, W. J. J.; Spek, A. L.; Veldman, N.; Wocadlo, S. *J. Chem. Soc., Dalton Trans.* **1998**, 3495−3499.

(33) Ramsamy, K.; Olsen, R. K.; Emery, T. *Synthesis* **1982**, 42−43.

(34) Borch, R. F.; Bernstein, M. D.; Durst, D. H. *J. Am. Chem. Soc.* **1971**, *93*, 2897−2904.

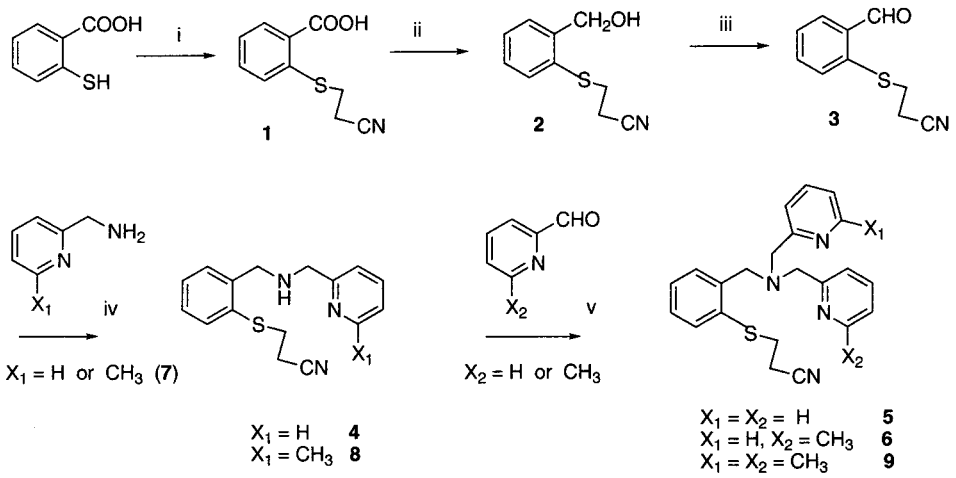

Reagents: i, (a) NaH/THF, (b) $BrCH_2CH_2CN$; ii, (a) EtOCOCl/TEA/THF, (b) $NaBH_4$; iii, MnO_2/CH_2Cl_2; iv, (a) MeOH, (b) $NaBH_4$; v, $NaBH_3CN/CH_3COOH$/MeOH.

Figure 1. Synthesis of the ligands **5**, **6**, and **9**.

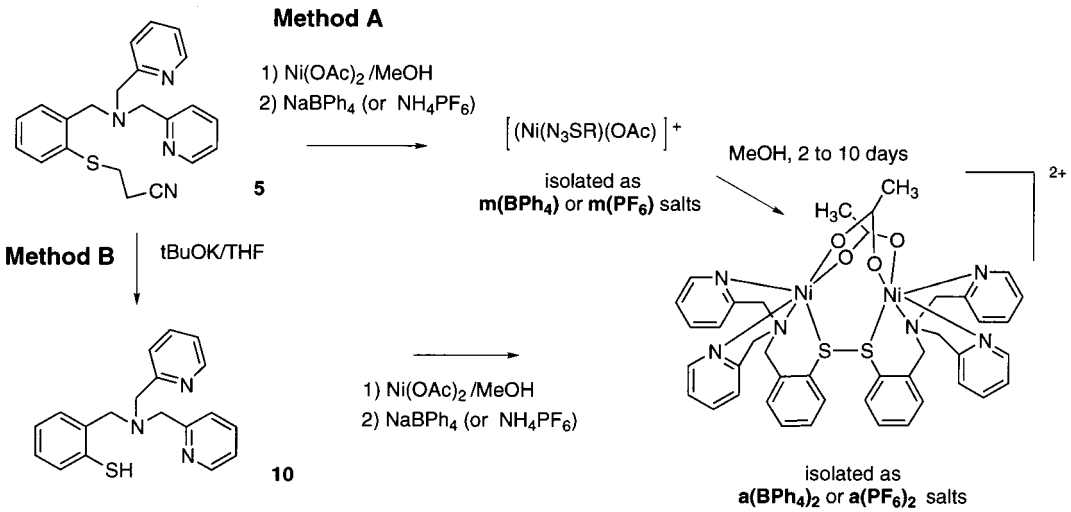

Figure 2. Mono- and dinuclear nickel(II) complexes prepared from ligand **5**.

and **9** (43% yield) are then isolated. It is worth noting that the same procedure with **3** and 2,2-bis(aminomethyl)-6-methylpyridine did not yield the desired tripod **9**.

Syntheses of the Nickel(II) Complexes. Different routes to the preparation of mono- and dinuclear nickel(II) complexes starting from ligand **5** are summarized in Figure 2, together with the complexes' nomenclature used in the rest of this work.

Dimeric Complexes: **Method A.** The Ni^{II} complexes are synthesized by mixing stoichiometric quantities of $Ni(OAc)_2 \cdot 4H_2O$ to a solution of the thio-protected ligand **5** in methanol, then the obtained blue solution is exposed to air at room temperature. A progressive color change from pale-blue to pale-green is observed over the period of a day. Upon stirring over an additional day and subsequent addition of $NaBPh_4$, the crude product precipitates. Filtration and recrystallization, by vapor diffusion of ethanol into an acetonitrile solution of this solid, affords pale-green crystals of X-ray quality. This crystalline material is dried in vacuo and affords pure **a(BPh$_4$)$_2$** ($[Ni_2(N_3SSN_3)(OAc)_2](BPh_4)_2$). Its formulation as a dinuclear complex is confirmed by X-ray crystal structure determination (vide infra) of the solvate **a(BPh$_4$)$_2$**$\cdot^1/_2[5(CH_3OH)\cdot(CH_3CN)\cdot(CH_3CH_2OH)]$. The two metal ions are six-coordinated and bridged by a disulfide group and by two additional bidentate acetates. Formation of this disulfide-bridged dinuclear nickel(II) complex involves in situ cleavage of the protecting cyanoethyl group upon complexation with the nickel salts and a subsequent oxidation process. Ni^{II}−S(disulfide) linkages are relatively rare: some mononuclear[35−37] Ni^{II} disulfide and bridging bis-(μ-disulfide)[38] compounds have been reported. **a(BPh$_4$)$_2$** is one of the two known examples[39] of μ-disulfide, bis(μ-acetato) dinuclear Ni^{II} complexes. The six-coordinated structure of **a-(BPh$_4$)$_2$** persists in solution as demonstrated by the electronic spectral properties: **a(BPh$_4$)$_2$** displays, in acetone solution, three broad absorption/shoulder bands with maxima at λ_{max} (nm, (ϵ, $M^{-1}\cdot cm^{-1}$)) 400 (sh), 575 (35), and 966 (46). These bands fall in the ranges 1430−770, 910−500, and 530−370 nm, respectively, assigned to the three spin-allowed transitions from the $^3A_{2g}(F)$ ground state to the next excited triplet states ($^3T_{1g}(P)$, $^3T_{1g}(F)$, and $^3T_{2g}(F)$) in octahedral Ni^{II} d^8 complexes.[40]

Dimeric Complexes: Method B. Alternatively (Figure 2), reaction of **5** with potassium *tert*-butoxide in THF affords, after workup, the pure free thiolate ligand **10**.[25] Reaction of **10** with

(35) Warner, L. G.; Ottersen, T.; Seff, K. *Inorg. Chem.* **1974**, *13*, 2529−2534.
(36) Warner, L. G.; Kadooka, M. M.; Seff, K. *Inorg. Chem.* **1975**, *14*, 1773−1778.
(37) Riley, P. E.; Seff, K. *Inorg. Chem.* **1972**, *11*, 2993−2999.
(38) Fox, S.; Stibrany, R. T.; Potenza, J. A.; Knapp, S.; Schugar, H. J. *Inorg. Chem.* **2000**, *39*, 4950−4961.
(39) Handa, M.; Mikuriya, M.; Okawa, H. *Chem. Lett.* **1989**, 1663−1666.
(40) Reference 11 pp 46−52.

$Ni(OAc)_2 \cdot 4H_2O$ in methanol under a nitrogen atmosphere and subsequent addition of $NaBPh_4$ induces the precipitation of a green powder. A crystalline material is obtained after purification. Spectroscopic and analytic data, in the solid state as well as in solution, proved this material to be identical to the former one prepared from method A. This study shows that complex **a(BPh$_4$)$_2$** could be obtained independently by two reaction pathways and gives evidence for the advantage of method A, which avoids isolation of the deprotected ligand prior to reaction with the nickel salts.

To investigate the spectroscopic properties of this complex (in particular the ^{1}H NMR assignment procedure described below), a series of dinuclear complexes were synthesized, including the PF_6 salt of the previous dimer, **a(PF$_6$)$_2$**, and complexes bearing methyl-substituted ligands **9** (**b(PF$_6$)$_2$**) and **6** (**c(PF$_6$)$_2$**).

Monomeric Complexes. To further explore the reactivity of the protected thiolate ligands with nickel salts, we have now focused on the isolation and characterization of compounds prior to the dimerization process. When the blue solutions obtained after the reaction of **5** with $Ni(OAc)_2 \cdot 4H_2O$ in methanol are stored at −20 °C and after $NaBPh_4$ or NH_4PF_6 are added, complex **m(BPh$_4$)** or **m(PF$_6$)** precipitates. The FAB spectra of these products show a peak at *m*/*z* 491 for the two complexes that are consistent with $[(N_3SR)Ni(OAc)]^+$ species. Elemental analysis and spectroscopic data also suggest an overall complex to anion 1:1 stoichiometry, thus leading to the formula $[(N_3SR)Ni(OAc)]BPh_4$ (or PF_6). The infrared spectra of these complexes measured in KBr disks show two strong features at ca. 1540 (1540) and 1426 (1420) cm^{-1} for **m(BPh$_4$)** (**m(PF$_6$)**), assigned to ν_{as}(COO) and to ν_s(COO), respectively. The ν_{as}(COO) features are similar to the values (range 1510−1550 cm^{-1}) described for metal complexes with bidentate nonbridging carboxylates and significantly differ from the values associated with a monodentate coordination mode (1600−1725 cm^{-1}). The ν_s(COO) features are also consistent with a bidentate nonbridging carboxylate coordination mode (range 1450−1470 cm^{-1}) described for such complexes.[41] These properties then suggest that **m(BPh$_4$)** and **m(PF$_6$)** complexes have one carboxylate group ligated to the nickel(II) in a bidentate mode. UV−visible spectroscopic data of dinuclear complexes **a(BPh$_4$)$_2$** and **a(PF$_6$)$_2$** and of mononuclear nickel(II) complexes **m(BPh$_4$)** and **m(PF$_6$)** are highly similar. λ_{max} (nm, (ϵ, M$^{-1}\cdot$cm^{-1})) for **m(BPh$_4$)**: 334 (148), 550 (10), 941 (16). λ_{max} (nm, (ϵ, M$^{-1}\cdot$cm^{-1})) for **m(PF$_6$)**: 408 (sh), 592 (6), 966 (4). This suggests an octahedral environment for the nickel center in mononuclear complexes **m(BPh$_4$)** and **m(PF$_6$)**. These bands are approximately half of the intensity of the corresponding bands in dimeric complexes, which is consistent with the presence of only one nickel per **m(BPh$_4$)** and **m(PF$_6$)** complex. Unfortunately attempts to characterize these materials by single-crystal X-ray studies have been unsuccessful so far. Nevertheless, ^{1}H NMR spectra (see Figure 4 below) afford a unique tool for discriminating between the two species. The solid compounds are air stable for months at room temperature, as well as in solution (acetone at −20 °C). Solutions in alcohol or acetonitrile can be handled in air at room temperature for short periods, but after some time, the dimeric cation is formed. The facile conversion of the mononuclear to the dinuclear systems can be controlled and both mono- and dinuclear complexes can be produced from the same ligands, depending only on the synthetic strategy. These ligands then offer unique opportunities in coordination chemistry.

(41) (a) Nakamoto, K. *Infrared and Raman Spectra of Inorganic and Coordination Compounds*, 4th ed.; Wiley: New York, 1986; pp 231−233. (b) Blake, A. J.; Danks, J. P.; Fallis, I. A.; Harrison, A.; Li, W.; Parsons, S.; Ross, S. A.; Whittaker, G.; Schröder, M. *J. Chem. Soc., Dalton Trans.* **1998**, 3969−3976.

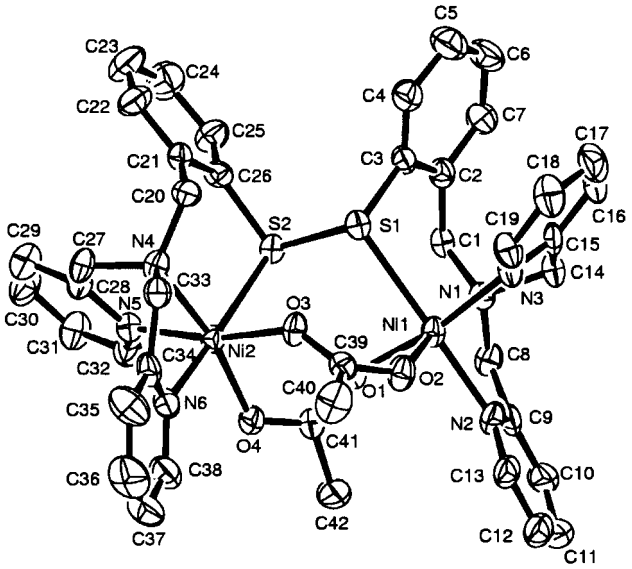

Figure 3. ORTEP plot of the dicationic unit **a** = $[Ni_2(C_{42}H_{42}N_6O_4S_2)]^{2+}$ showing only one (**a$_1$**) of the two independent entities **a$_1$** and **a$_2$** with atom labels and numbering scheme. Hydrogens are omitted for clarity. Ellipsoids are drawn at the 35% probability level.

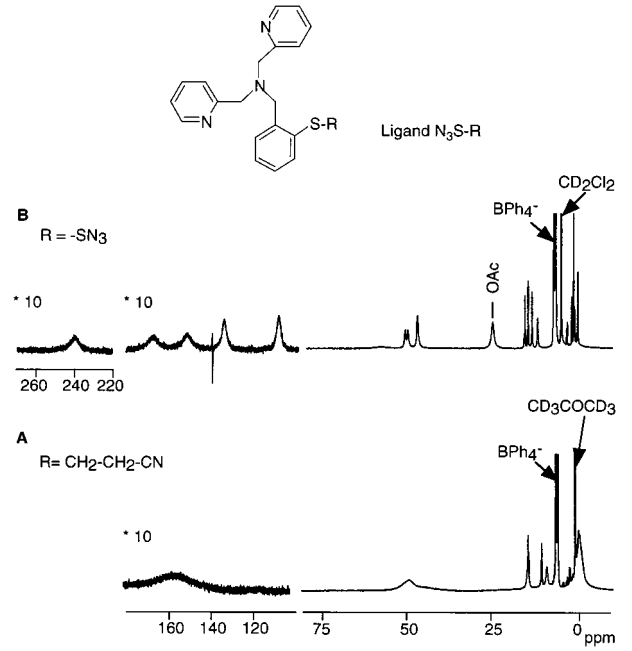

Figure 4. ^{1}H NMR spectra at 298 K of (A) the mononuclear complex **m(BPh$_4$)** in acetone-d_6 and of (B) the dinuclear complex **a(BPh$_4$)$_2$** in CD_2Cl_2. Solutions are 10^{-2} M in complex and spectra are recorded at a repetition rate of 2 s^{-1}. Resolution is enhanced in the upfield portion of the spectra through acquisition on a limited 48 kHz bandwidth.

Description of a(BPh$_4$)$_2$ Crystal Structure. The complex **a(BPh$_4$)$_2$** was isolated from methanol and recrystallized from acetonitrile/ethanol. The unit cell contains two crystallographically independent $[Ni_2(C_{42}H_{42}N_6O_4S_2)](BPh_4)_2 \cdot {}^1/_2$solvate entities, where solvate stands for five methanol, one ethanol, and one acetonitrile solvent molecules. Each cationic unit, one of which (**a$_1$**) is shown in Figure 3, consists of two Ni atoms bridged by two acetate ions and a disulfide group. The hexacoordination sphere of each nickel atom is completed by one amino- and two pyridyl-nitrogen atoms. Selected bond distances and angles are reported in Table 1 and show no

significant difference between the two nickel dimers. Overlaying the two dimeric structures $\mathbf{a_1}$ (Figure 3) and $\mathbf{a_2}$ (see Supporting Information) with the Insight II software[26c] furthermore leads to a high degree of homology between the two crystallographic entities. In fact, the two structures mainly differ on pyridyl aromatic ring orientation, which infers slight interatomic elongations and angle distortions due to steric constraints. Superimposing Ni1, O1, O2, N1, N2, and N3 atoms in $\mathbf{a_1}$ with respectively Ni4, O7, O8, N10, N11, and N12 in $\mathbf{a_2}$ yields to a 0.0338(1) root-mean-square deviation for the whole molecule distances. This emphasizes the lack of significant differences between the two dimers. Superposition of Ni1 and Ni3 in the same fashion gives rise to a very similar, although slightly higher, 0.0353(1) root-mean-square value. This closely relates the two nickel centers in each dimer, which can be emphasized through the definition of a pseudo-C_2 axis passing through the midpoint of the Ni···Ni and of disulfide bridge. The X-ray crystal structure of $\mathbf{a(BPh_4)_2}$ can then be considered as highly symmetrical despite the lack of a true crystallographic symmetry element.

Inside each dimer, the Ni atoms are separated by 4.243(1) Å in $\mathbf{a_1}$ and 4.299(2) Å in $\mathbf{a_2}$, which is typical of the intermetallic distances measured in octahedral Ni_2^{II}−S(sulfide) complexes (4.220(3)[38] and 4.134(2) Å[39]). The observed S−S bond lengths in $\mathbf{a(BPh_4)_2}$ (2.073(2) Å for $\mathbf{a_1}$ and 2.080(2) Å for $\mathbf{a_2}$) also fall in the 2.015(6)−2.108(6) Å range mentioned by Fox et al.[38] They are nevertheless slightly longer than the 2.056(3) Å value in a similar dinuclear octahedral Ni^{II} compound[39] with an aliphatic disulfide bridge and to the 2.039(7) or 2.040(3) Å values in mononuclear complexes with nonbridging disulfide groups.[37] It can be noted that the Ni−S−S−Ni atoms are not coplanar, with a torsion angle of 72.67(7)° in $\mathbf{a_1}$ and 69.75(7)° in $\mathbf{a_2}$. The bridging acetate ligands adopt a typical "syn-anti" conformation, with Ni−O distances ranging from 1.981(4)−2.010(3) Å to 2.042(4)−2.067(4) Å. These features have also been observed in other bis(μ-acetato)−dinuclear Ni^{II} paramagnetic complexes.[39,42−44]

The coordination geometry around each nickel is a distorted octahedron. Nevertheless, angles involving the Ni atoms show little deviation from the theoretical angles, emphasizing the quasiregularity of the polyhedra. As a matter of fact, the largest deviations are encountered for O7−Ni4−N12 (166.2°, 13.8° deviation) and N4−Ni2−N6 (79.8°, 10.2° deviation). With respect to distances between the metal center and bound heteroatoms, the Ni−S bonds (2.524(2) and 2.527(2) Å for $\mathbf{a_1}$, and 2.513(2) and 2.517(2) Å for $\mathbf{a_2}$) are elongated; they are indeed much longer than the other Ni−O or Ni−N distances, which all fall in the range 1.981(4)−2.100(4) Å. These results are however consistent with the Ni−S distances observed in high-spin six-coordinated Ni^{II} complexes bearing disulfide ligands, including monodentate disulfide (2.470(5),[35] 2.456(2),[36] and 2.472(2) Å[37]) and bridging disulfide (2.503(3)[39] and 2.519(4)−2.565(4) Å[38]). In paramagnetic Ni−SR_2 complexes, the reported Ni−S bond lengths are in the range 2.32−2.52 Å[45] as in bridging alkyl- or arylsulfide (2.518(1)−2.541(1) Å[18] and 2.499(4)−2.482(4) Å[46]). Interestingly, the Ni−S in 2-mercaptoethanol-inhibited urease (average Ni−S distance 2.36 Å[7]) falls in the same range. The Ni−N distances (2.028(5)−2.100(4) Å) are characteristic of octahedral high-spin Ni^{II} [47] and are indeed longer than in square-planar Ni^{II} complexes.[45a] The weaker Ni−N interactions for tertiary amine (2.051(5)−2.100(4) Å) relative to pyridine amine (2.028(5)−2.074(5) Å) in $\mathbf{a_1}$ and $\mathbf{a_2}$ are typical.

Magnetic Susceptibility Studies. The magnetization properties of $\mathbf{a(BPh_4)_2}$ have been studied to evaluate the magnetic interactions between the two nickel atoms. The temperature dependence of the product of the molar susceptibility by temperature is illustrated in the Supporting Information (Figure 2S). The data are roughly constant with $\chi T \sim 2.54$ cm^3·K·mol^{-1} when the temperature is lowered from 300 to 100 K. This value is close to that expected (2.42 cm^3·K·mol^{-1}) for two uncoupled $S = 1$ spins arising from nickel ions with $g = 2.2$. At lower temperatures, χT shows an increase up to 3.3 cm^3·K·mol^{-1} (value at 7 K) at 0.5 T. Such a behavior is characteristic of a ferromagnetically coupled nickel pair. The decrease observed at very low temperatures is essentially due to saturation effects, but also to moderate zero-field splitting, as can be seen on a magnetization versus $\beta H/k_B T$ representation (where H is the applied magnetic field).

The following equations, based on the Hamiltonian $\hat{H}$, were used to fit the magnetic data:

$$\hat{H} = -2J\hat{S}_1.\hat{S}_2 + \beta\vec{H}.\tilde{g}.\hat{S} \qquad (1)$$

$$\chi T = \frac{3g^2}{4}\frac{\exp\frac{2J}{k_B T} + 5\exp\frac{6J}{k_B T}}{1 + 3\exp\frac{2J}{k_B T} + 5\exp\frac{6J}{k_B T}} + 2\mathrm{TIP}\cdot T \qquad (2)$$

The first term represents the contribution of the coupled pair with its g factor and its exchange interaction (J). The last term represents the contribution of the temperature independent paramagnetism (TIP) of each nickel atom. The best least-squares fit was obtained using the data at the four magnetic fields together, in the valid temperature domain, and led to the following values: $J = 2.5(7)$ cm^{-1}, $g = 2.19(6)$, TIP = 200(200) × 10^{-6} cm^3·mol^{-1}.

More sophisticated equations were used including zero-field splitting, inter-dimer exchange interaction, and paramagnetic impurities.[48] However, in the temperature range used for the fitting procedure, zero-field splitting and inter-dimer effects (the distance between two Ni atoms of two distinct dimers is d_{min} = 8.699 Å) should be very small and will not significantly change the obtained J value. Moreover, the saturation effects, which are important at low temperature, will be superimposed to these interactions and eq 2 is no more valid.

Only one nickel(II) dimer with a disulfide and two acetate bridges has been structurally and magnetically characterized so far.[39] A Curie−Weiss law was observed. However, the temperature domain explored was limited (100−300 K) and therefore the small ferro- or antiferromagnetic interaction, if existing, could not be measured. A nickel(II) dimer with two disulfide bridges recently has been structurally and magnetically characterized by Fox et al.[38] An antiferromagnetic interaction was described with $J = -13.0(2)$ cm^{-1}. This complex presents some similarities to $\mathbf{a(BPh_4)_2}$: Ni···Ni distances (4.220 Å for

(42) Volkmer, D.; Hörstmann, A.; Griesar, K.; Haase, W.; Krebs, B. *Inorg. Chem.* **1996**, *35*, 1132−1135.
(43) Buchanan, R. M.; Mashuta, M. S.; Oberhausen, K. J.; Richardson, J. F. *J. Am. Chem. Soc.* **1989**, *111*, 4497−4498.
(44) Chaudhuri, P.; Küppers, H.-J.; Wieghardt, K.; Gehring, S.; Haase, W.; Nuber, B.; Weiss, J. *J. Chem. Soc., Dalton Trans*. **1988**, 1367−1370.
(45) (a) Bohle, D. S.; Zafar, A.; Goodson, P. A.; Jaeger, D. A. *Inorg. Chem.* **2000**, *39*, 712−718. (b) Cha, M.; Gatlin, C. L.; Critchlow, S. C.; Kovacs, J. A. *Inorg. Chem.* **1993**, *32*, 5868−5877 and references therein.
(46) Baidya, N.; Olmstead, M.; Mascharak, P. K. *Inorg. Chem.* **1991**, *30*, 929−937.
(47) Mikuriya, M.; Handa, M.; Shigematsu, S.; Funaki, S.; Fujii, T.; Okawa, H.; Toriumi, K.; Koshiba, T.; Terauchi, H. *Bull. Chem. Soc. Jpn.* **1993**, *66*, 1104−1110.
(48) Ginsberg, A. P.; Martin, R. L.; Brookes R. W.; Sherwood, R. C. *Inorg. Chem.* **1972**, *11*, 2884−2889.

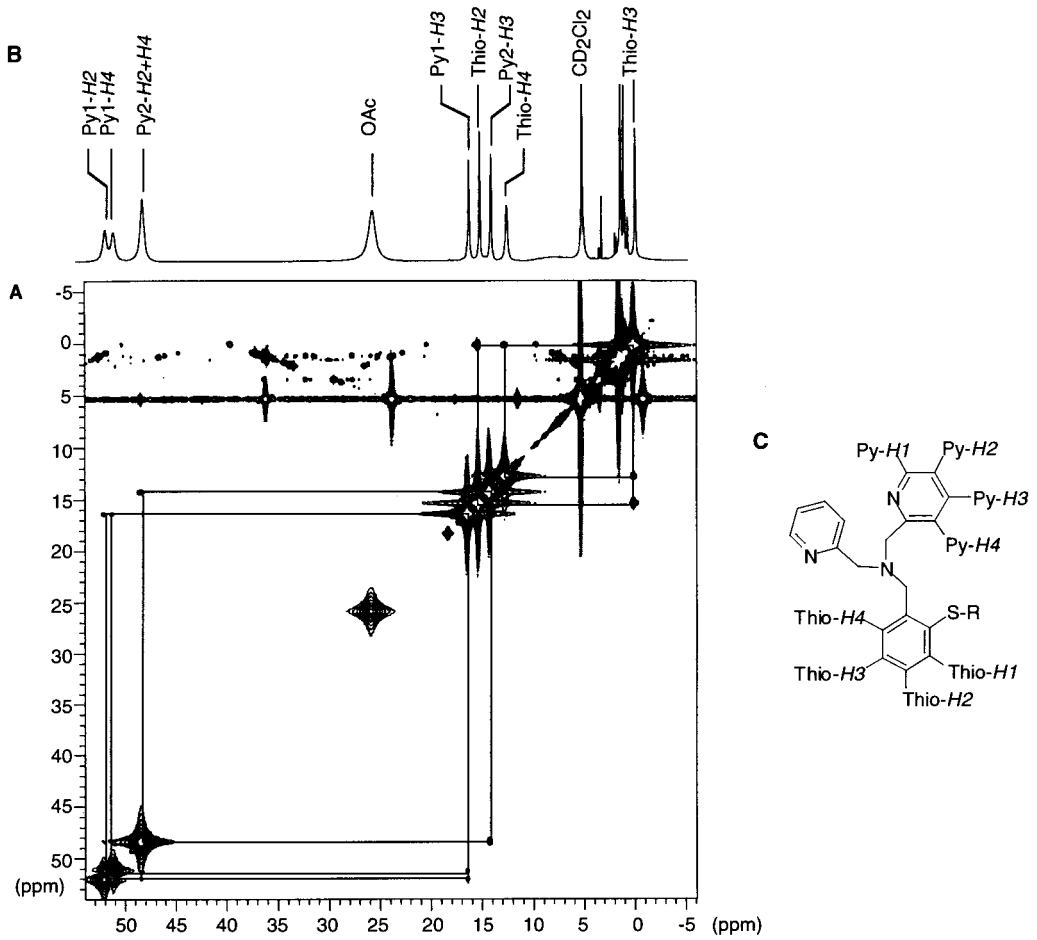

Figure 5. (A) ^{1}H 1D and (B) magnitude COSY spectra of **a(PF$_6$)$_2$** in CD_2Cl_2 at 293 K. The spectrum was obtained using 4096 t_2 and 512 t_1 data points. Nonshifted sinebell apodization function and zerofilling to 4K t_2 × 1K t_1 data points prior to Fourier transform were used during data processing. No symmetrization was performed on the resulting 2D spectrum, due to noise in the t_1 dimension. Pyridyl and thiophenolic spin systems are shown. Part C reproduces the ligand numbering scheme used for signal assignment.

Fox's complex and an average value of 4.271 Å for **a(BPh$_4$)$_2$**), a bridging disulfide. Nevertheless the overall symmetry of each complex is rather different. A better orbital overlap in the Fox dimer, which is favorable to a superexchange pathway, and consequently, to an antiferromagnetic interaction, may be responsible for the sign and intensity difference observed in the *J* values. Further studies such as theoretical calculations should be useful for understanding the magnetostructural correlations in disulfide-bridged bis-nickel(II) complexes.

^{1}H NMR General Features. ^{1}H NMR spectra of dinuclear **a(BPh$_4$)$_2$** and mononuclear **m(BPh$_4$)** complexes, illustrated in Figure 4, show striking differences. The monomeric species **m-(BPh$_4$)** (Figure 4A) present few and extremely broad resonances: a maximum of seven resonances are detected and line widths up to 16 000 Hz are observed. In the case of the **a(BPh$_4$)$_2$** dimer (Figure 4B), 16 very well resolved isotropically shifted resonances can be identified on the ^{1}H NMR spectrum on a 300 ppm spectral window with 2000 Hz maximum line width. ^{1}H NMR features such as smaller hyperfine shifts and larger line width could thus be considered as the spectroscopic signature for high-spin nickel(II) monomers vs high-spin nickel-(II) dimers, at least in a mixed N/S/O coordination mode. Taking advantage of the versatility of ligands N_3SR (Scheme 1), resonances assignment strategies, impact of magnetic coupling on the ^{1}H NMR spectral properties of high-spin nickel(II) compounds, and relaxation mechanisms are addressed in the following sections.

^{1}H NMR Resonance Assignment Strategy for a(BPh$_4$)$_2$. The high similarity between the two dimers **a$_1$** and **a$_2$** identified in the crystallographic unit cell is expected to yield to the detection of a unique dimer in solution through ^{1}H NMR studies. Furthermore, the presence of a pseudo-C_2 axis in each dimer's crystal structure suggests that the complex may adopt a 2-fold symmetry in dichloromethane solution. This is fully consistent with the identification of 16 resolved resonances only, on the ^{1}H NMR spectrum of **a(BPh$_4$)$_2$** in CD_2Cl_2 at 298 K (Figure 4B). As a starting point for assignment, integration of every resolved signal can be considered, thus allowing the unambiguous identification of the μ-acetato methyl group resonance at 25.59 ppm. This assignment is furthermore confirmed through acetate vs chloride substitution (data not shown).

COSY experiments are particularly adapted to mapping spin−spin coupling networks in diamagnetic samples and cross-peak intensities are dictated by the importance of the nuclear scalar *J*-coupling constant value. In paramagnetic complexes, however, its success can severely be hampered by the following factors: intrinsic T_2 relaxation time,[10] spectral width and related 90° pulse efficiency, and presence of diamagnetic species. Taking these limitations into account, a magnitude COSY spectrum with decent signal-to-noise ratio (Figure 5) could be obtained on a 34 kHz window for a **a(PF$_6$)$_2$** sample in CD_2Cl_2 at 293 K with 2048 scans. It must be noted that chemical shift and resonance line width of the complex cation **a** are essentially insensitive to anion substitution, which appears to be essential. The upfield

Table 2. NMR Parameters in CD_2Cl_2 at 293 K and Crystal Structure Data for the Dimeric Species **a(BPh$_4$)$_2$**

resonance assignment		δ (ppm)[a]	$\Delta\nu_{1/2}$ (Hz)[b]	$Ni_1\cdots H$ (Å)[c]	$Ni_2\cdots H$ (Å)[c]	angle (deg)[d]	T_{1exp} (ms)[e]	T_{1calc} (ms)[f]
Py1+2	*H1*	155.03	1484	3.14[g]	6.01[g]		0.16	0.15[g]
		171.78	2027	3.12[h]	5.77[h]		0.14	0.15[h]
Py1	*H2*	52.04	238	5.07[g]	7.76[g]		3.09	2.55[g]
	H3	16.30	60	5.71[g]	8.60[g]		7.57	5.16[g]
	H4	51.20	554	4.87[g]	7.95[g]		2.75	2.05[g]
Py2	*H2*	48.38	204	5.05[h]	7.80		3.13	2.50[h]
	H3	14.15	55	5.71[h]	9.06		8.00	5.27[h]
	H4	48.38	204	4.89[h]	8.66		3.13	2.14[h]
Thio	*H1*	$\sim$ 5.32[i]		4.90	5.83			1.65
	H2	15.33	44	6.48	7.98		10.35	9.29
	H3	0.09	43	6.61	8.79		11.41	11.41[f]
	H4	12.36	99	5.28	7.85		3.88	3.20
CH_2 H_{eq}	Py *trans*[g]	137.80	1069	3.69	7.01	161.30	0.58	0.40
	Py *cis*[h]	245.82	1790	3.72	7.49	151.13	0.60	0.42
	Thio	112.28	1045	3.86	6.45	167.73	0.62	0.51
CH_2 H_{ax}	Py *trans*[g]	$\sim$7.5[j]	1092	3.07	5.66	79.16	0.17	0.13
	Py *cis*[h]	0.09[i]		3.27	7.41	89.51		0.20
	Thio	59.29		3.06	4.93	49.10		0.13
OAc	CH_3	25.99	351	4.20	4.56		1.10	0.55

[a] Observed chemical shifts, in ppm, referenced to residual solvent resonance at 5.32 ppm. [b] Line width of each resolved resonance. [c] Average distances obtained from the four slightly nonequivalent proton positions in the crystal structure unit cell. These distances are measured within the Insight II program. Ni_1 points out the Ni atom closer to the considered proton. [d] Angles considered are $Ni_1-N-C-H$ angles and are measured within the Insight II program. [e] T_1 values obtained from the monoexponential fitting procedure of the inversion−recovery data on 36 array values. A comparison of three independently acquired data sets yields a maximal 2.5% error on the reported values. [f] T_1 values calculated on the basis of a model taking into account a predominant dipolar relaxation mechanism, arising from two paramagnetic Ni^{II} S = 1 centers with negligible magnetic interactions. The relaxation rates (T_{1calc}^{-1}) are calculated on the basis of crystal structure data (giving the r_{Ni-H} values) with respect to that of a reference resonance (T_{1ref}^{-1}), according to the following equation: $T_{1calc}^{-1} = T_{1ref}^{-1}[(r_{Ni1-H}^{-6} + r_{Ni2-H}^{-6})/(r_{Ni1-H}^{-6} + r_{Ni2-H}^{-6})_{ref}]$ (see ref 50). The Thio-*H3* proton is used as a reference in this calculation, with $T_{1ref} = 11.41$ ms, $r_{Ni1-H} = 6.61$ Å, and $r_{Ni2-H} = 8.79$ Å. A change in the reference implies different T_1 values, but highly similar qualitative agreement between the experimental and calculated values. This fitting procedure gives better results than other described methods, involving the average distance between the metal centers and the proton of interest in a point dipole approximation.[20, 22] [g] Structural data measured for the pyridyl ring in a respectively trans position with respect to the thiophenolic anchoring on the metal. [h] Structural data measured for the pyridyl ring in a respectively cis position with respect to the thiophenolic anchoring on the metal. [i] Resonances identified on the basis of a temperature study that can solve fortuitous overlap. [j] Proposed chemical shift value based on spectral comparison with **a(PF$_6$)$_2$**.

portion of the spectrum exhibits a three-spins system (15.36, 12.75, and 0.12 ppm) that unambiguously assigns the corresponding protons to one of the aromatic rings. Two additional similar spin−spin connectivity patterns, involving the resonances at 52.05, 51.24, and 16.42 ppm (48.40 and 14.27 ppm, respectively), are outlined in the downfield portion of the spectrum. The resonance at 48.40 ppm integrates for two protons and results from coincidental degeneracy, which can be raised with solvent change (to DMSO for example). These spin systems then account for parts of all three aromatic rings. It must be noted that the Ni−S bond (average distance 2.520 Å) is expected to be weaker than the Ni−N bond (average distance 2.064 Å). Assuming a major contribution of the contact shift to the overall hyperfine shift, like in nickel(II) monomers,[49] the most upfield shifted three-spin system can consequently tentatively be assigned to the thiophenolic ring protons. Furthermore, spin−spin coupling to aromatic *H1* may occur beyond detection due to the proximity of these protons to the nickel center and enhanced resulting relaxation properties. This leads to the following specific assignment: resonances at 16.42, 14.27, and 0.12 ppm correspond respectively to Py1-*H3*, Py2-*H3*, and Thio-*H3*. The subsequent *H3*-to-*H2* and *H3*-to-*H4* coupling schemes then result in the observed connectivities. These assignments are transposable to **a(BPh$_4$)$_2$** and are summarized in Table 2 (it must be noted that labels 1 and 2 are arbitrarily proposed for one or the other of the pyridyl rings).

Further assignments cannot be made without specific chemical substitution, or interpretation of proton longitudinal relaxation measurements in correlation with distances between Hs and the nickel centers. Directed chemical substitution, especially at the key Py-*H1* position, is considered first and is monitored in Figure 6. The substitution of Py-*H1*s in **a(PF$_6$)$_2$** by methyl groups in **b(PF$_6$)$_2$** results in the disappearance of the 1200 Hz broad resonances at 171.43 and 155.43 ppm (Figure 6A) and appearance of two new resonances, integrating for three protons each, at −8.11 and −10.25 ppm (Figure 6B). The magnetic inequivalence of the two pyridyl *H1*s resonances originates in differences in contact and dipolar shifts for the pyridyl in the cis vs trans position with respect to the thiophenolic ring. The Py-*H1* signal detected at 171.43 ppm in **a(PF$_6$)$_2$** probably corresponds to the most upfield-shifted methyl resonance at −10.25 ppm in **b(PF$_6$)$_2$**, but no specific assignment can nevertheless be proposed at the present stage. The present partial assignment is nevertheless confirmed by the detection of both sets of resonances in the dissymmetrically substituted **c(PF$_6$)$_2$** complex (Figure 6C). Furthermore, four resonances in a 1:1:1:1 ratio are detected in the later case in the methyl upfield region. Such observation is consistent with the nonselective formation of four stereoisomers upon complexation: the cis-cis, trans-trans, cis-trans, and trans-cis isomers, cis or trans referring to the position of the methylated ring with respect to the thiophenolic groups.

Specific chemical substitution at the Py-*H1* position also provides additional evidence to former assignments. Comparison of COSY spectra collected under the same conditions (see Supporting Information), as well as 1D-temperature and relaxation studies, for **a(PF$_6$)$_2$**, **b(PF$_6$)$_2$**, and **c(PF$_6$)$_2$** clearly identifies the resonances at 15.36, 12.75, and 0.12 ppm in **a(PF$_6$)$_2$** to respectively Thio-*H2*, Thio-*H4*, and Thio-*H3*, as well as the presence of a fast relaxing resonance under the residual CD_2Cl_2 solvent peak at 5.32 ppm to Thio-*H1*. Present assignments are then transposed to **a(BPh$_4$)$_2$** and reported in Table 2.

(49) Reference 11 pp 56−60.

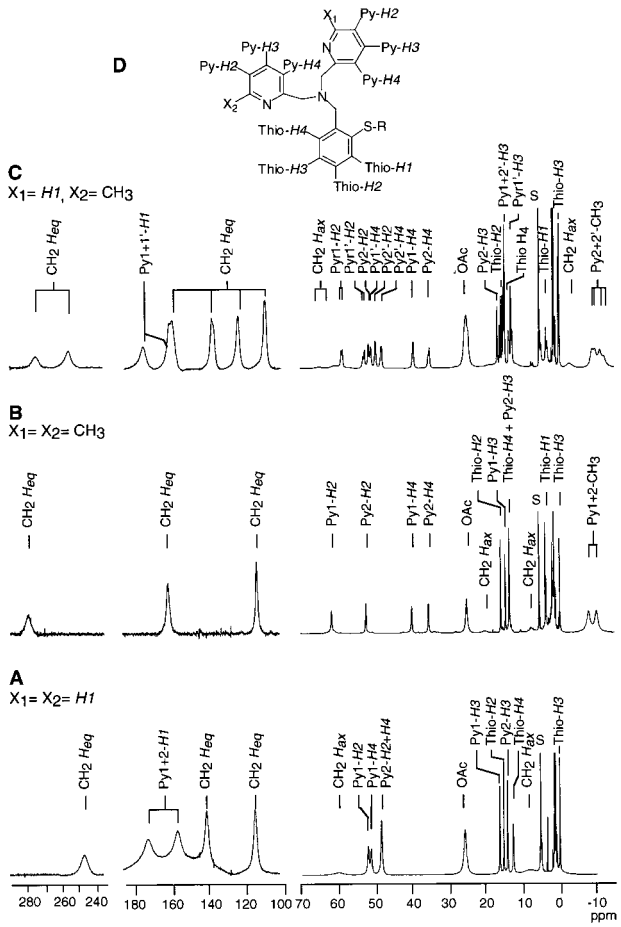

Figure 6. Portions of the ^{1}H NMR spectra in CD_2Cl_2 at 293 K of the dinuclear complexes bearing different chemical substitutions on the ligand: (A) $X_1 = X_2 = H1$, **a(PF$_6$)$_2$**; (B) $X_1 = X_2 = CH_3$, **b(PF$_6$)$_2$**; (C) $X_1 = H1$ and $X_2 = CH_3$, **c(PF$_6$)$_2$**, according to the ligand numbering scheme shown in part D. The solvent residual signal at 5.32 ppm is labeled S on each spectrum. All solutions are 5×10^{-3} to 10^{-2} M in dinuclear complex.

At this point, pyridyl and thiophenolic ring assignments, together with acetate identification, leave four resolved signals in the downfield spectral window of the **a(BPh$_4$)$_2$** spectrum (at 245.82, 137.80, 112.28, and 59.29 ppm). These resonances must consequently arise from methylene protons. According to literature,[50,51] geminal methylene protons involved in the chelate ring experience significantly different hyperfine shift (contact shift) and relaxation times (dipolar relaxation). Equatorial-like protons (i.e. methylene protons located further away from Ni^{II} with a dihedral angle Ni−N−C−H closer to 180°) are consequently expected to show longer relaxation times and greater downfield hyperfine shift with respect to their geminal partners CH_2 H_{ax}. Three of the unassigned resonances with large downfield isotropic hyperfine shifts (>100 ppm) and enhanced 0.7−0.9 ms T_1 and 0.3−0.6 ms T_2 relaxation times are then considered likely candidates. More detailed specific assignment of these protons implies T_1 measurement analysis, in correlation with the crystal structure considerations reported in Table 2. Using these data, the expected δ_{ax}/δ_{eq} ratio is calculated for each methylene group, according to the following empirical formula proposed by Ho and Reilley:[51]

$$\frac{\delta_{ax}}{\delta_{eq}} = \frac{\cos^2\theta}{\cos^2(120+\theta)} = \begin{array}{r} 4.4 \times 10^{-1} \text{ for thiophenolic methylene} \\ 4.0 \times 10^{-2} \text{ for } \textit{trans}\text{-pyridyl methylene} \\ 9.7 \times 10^{-5} \text{ for } \textit{cis}\text{-pyridyl methylene} \end{array} \quad (3)$$

where θ states for the Ni−N−C−H_{ax} dihedral angle, δ_{ax} and δ_{eq}, are the observed chemical shift for axial- and equatorial-like methylene protons CH_2 H_{ax} and H_{eq}, and trans and cis designate the position of the pyridyl ring bound to the methylene of interest with respect to the thiophenolic anchor on the nickel center. According to the above results and relaxation data in Table 2, Thio CH_2 H_{eq} is expected to show the smaller isotropic hyperfine shift and the longer T_1 value. It is therefore assigned to the resonance at 112.28 ppm (Figure 4B). Furthermore, this resonance remains unshifted upon chemical substitution on the pyridyl ring (Figure 6A,B), which is in complete agreement with the present assignment. According to the δ_{ax}/δ_{eq} ratio, Thio CH_2 H_{ax} (Ni···H distance = 3.06 Å) is expected to resonate at 49.40 ppm and to present a 0.13 ms T_1 relaxation time. The detected peak at 59.29 ppm, with $T_1 = 0.17$ ms, is then a very likely candidate. Assuming that the pyridyl methylene CH_2 H_{ax} protons fall in the diamagnetic window, the above criteria lead to the identity of the resonances at 245.82 and 137.80 ppm respectively as *cis*- and *trans*-Py-CH_2 H_{eq}. Their corresponding geminal partners are then expected to resonate at 5.51 and 0.02 ppm and to present 0.13 and 0.20 ms longitudinal relaxation times. Interestingly, the ^{1}H NMR spectrum of complex **a(PF$_6$)$_2$** at 293 K, reported in Figure 6A, shows a resonance at 8.58 ppm ($T_1 = 0.15$ ms) and a temperature study of **a(BPh$_4$)$_2$** reveals an additional resonance at 0.09 ppm at 263 K, for which chemical shift and the slope of the $\delta = f(1/T)$ plot are consistent with its assignment to *cis*-Py-CH_2 H_{ax}. The good agreement between these observations and the above predictions is considered strong evidence in favor of the assignment of pyridyl CH_2 H_{ax}.

Complete assignment and spectroscopic properties (observed chemical shift, longitudinal relaxation times, and line width) of each resonance are reported in Table 2 for complex **a(BPh$_4$)$_2$**. These results have been obtained through a combination of 2D methods, directed chemical substitution, and analysis of T_1 data, as well as the chemical shift temperature dependence study. Similar strategy yields the complete assignment of **a(PF$_6$)$_2$**, **b-(PF$_6$)$_2$**, and **c(PF$_6$)$_2$** ^{1}H NMR resonances that is provided in the Supporting Information.

^{1}H NMR Resonance Assignment Strategy for m(PF$_6$) or m(BPh$_4$). The above strategy assignment remains inefficient for the monomer species **m(PF$_6$)** or **m(BPh$_4$)**, due to extreme T_1 and especially T_2 relaxation times. Nevertheless, a tentative assignment can be proposed on the basis of T_1 comparisons between the monomer and the dimer, providing a conservative geometry around the nickel center, as suggested by other spectroscopic methods except NMR. The resonances at 15.26 ($T_1 = 6.99$ ms) and 11.41 ppm ($T_1 = 9.85$ ms) must arise from aromatic *H3* protons and/or Thio-*H2*, while signals at 48.85 ($T_1 = 2.27$ ms) and 10.07 ppm ($T_1 = 2.90$ ms) rather correspond to aromatic *H2* or *H4* protons (Figure 4A). On the other hand, resonances at 158.54 ($T_1 = 0.18$ ms) and −2.96 ppm ($T_1 = 0.55$ ms) may be respectively assigned to methylene groups (or aromatic *H1* protons) and the acetate group. Observed T_1 values are overall slightly shorter than the corresponding values in the

(50) Ming, L.-J.; Jang, H. G.; Que, L., Jr. *Inorg. Chem.* **1992**, *31*, 359−364.

(51) Holm, R. H.; Hawkins, C. J. *NMR of paramagnetic molecules: Principles and applications*; La Mar, G. N., Horrocks, W. DeW., Jr., Holm, R. H., Eds; Academic Press: New York, 1973; pp 243−332 and references therein.

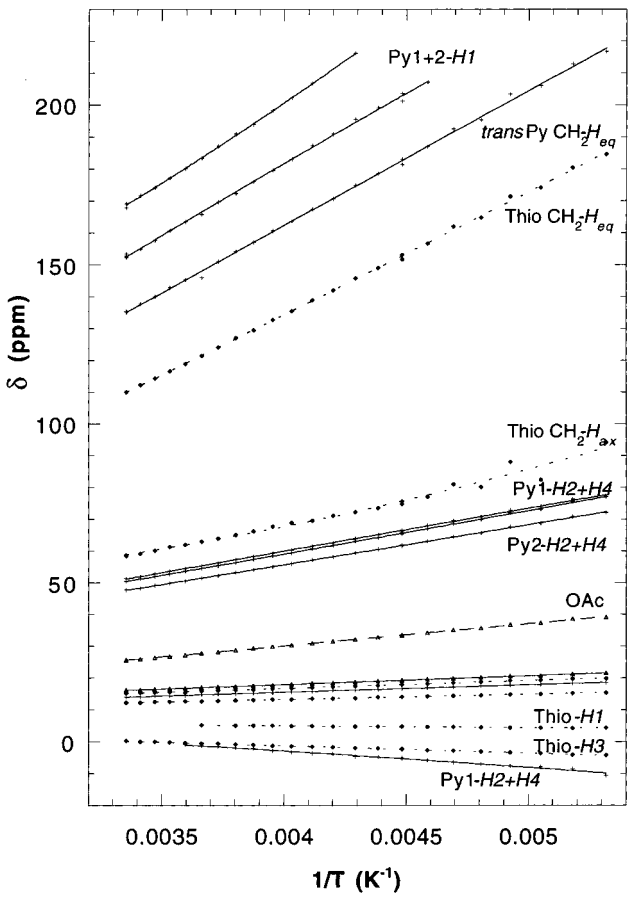

Figure 7. Observed chemical shift dependence vs reciprocal temperature for resonances of **a(BPh$_4$)$_2$** in CD_2Cl_2. Signs and lines show respectively experimental and second-order polynomial square fit data for all assigned resonances, except the *cis*-pyridyl CH_2 H_{eq} signal. (+) Filled lines emphasize the behavior of pyridyl ring and methylene protons, (♦) dotted lines the behavior of the thiophenolic ring and methylene protons, and (Δ) broken lines the behavior of acetate protons.

dinuclear species. Enhancement of the monomer vs dimer relaxation rates is even more sensitive for the transversal relaxation rates. As an example, the resonance at 158.54 ppm shows the same T_1 value as Py-*H1* in the dimeric species, while the line width of the corresponding peaks differs by a factor of 8. These observations are consistent with the presence of a relaxation cooperative effect in dimeric vs monomeric compounds. This effect is similar to results previously reported on copper(II) model complexes.[22]

Hyperfine Shifts in Nickel(II) Dimers. Chemical shift of every ^{1}H NMR dimer resonance is significantly temperature sensitive. Experimental data over the temperature range 188−298 K are reported in Figure 7 for **a(BPh$_4$)$_2$** in CD_2Cl_2, showing a typical Curie behavior. Fits of reasonably good quality (correlation coefficients greater than 0.985 for all resonances and greater than 0.999 in most cases) can be obtained using a linear Curie law and are reported in Table 3. Slopes highly correlate with the magnitude and sign of the hyperfine shift in each case ($\delta_{hf} = \delta - \delta_{dia}$, where δ is the observed chemical shift). A comparison of the slopes for the two methylene geminal partners (16.5×10^3 ppm.K for Thio-CH_2 H_{ax} and 38.3×10^3 ppm.K for Thio-CH_2 H_{eq}) furthermore emphasizes the absence of correlation between the magnitude of the slope and the Ni···H distances (respectively 3.06 and 3.86 Å). This is a strong evidence in favor of a highly predominant contact contribution to chemical shift. On the contrary, some of the intercepts significantly differ from the expected[8] diamagnetic shift (see, for example, Py1+2-*H1*, Py- and Thio-CH_2s), thus suggesting small deviations to the Curie law.

Such deviations can be understood considering the presence of one (or more) low-lying excited state(s), where the differences in energy between ground and excited levels are of the order of thermal energy k_BT. In the particular case of **a(BPh$_4$)$_2$**, each nickel center lays in a pseudo-octahedral environment of four different ligand atoms. The ligand field theory leads to a $^3A_{2g}$ orbitally nondegenerate ground state for each nickel atom and the spin levels may be split to a small extent through the zero-field splitting D, usually on the order of 0−60 cm^{-1} in mononuclear complexes.[52] Such contribution also stands for dinuclear species, although the magnitude of the zero-field splitting may differ from the mononuclear ones. According to Kurland and McGarvey,[53] this implies, for a spin $S = 1$ when $D \ll k_BT$, a T^{-1} but also additional T^{-2} temperature dependence of the hyperfine chemical shift. In the dinuclear complexes studied, the two nickel atoms are furthermore ferromagnetically spin-coupled to each other and the resulting J coupling constant is an additional source for energy level splitting. If J is on the order of a few cm^{-1}, the $S' = 0$, 1, 2 energy levels (S' is the total dimer spin-state) are expected to be significantly populated at room temperature. According to a very elegant study by Shokheriev and Walker,[54] this also implies an additional T^{-2} contribution to fitting expressions of observed chemical shift. To target the potential importance of J and/or D in dinuclear nickel(II) complexes and deviations to Curie law, observed chemical shifts versus the inverse temperature are processed using a second-order polynomial fitting expression. No significant improvement of fit quality can be observed from this procedure and correlation coefficients remain rather insensitive to the type of fitting expression retained. Nevertheless, very good fits, reported in Table 3, can be obtained in the latter procedure that give intercepts identical to the expected diamagnetic shift. T^{-1} and T^{-2} coefficients are obtained with a 10% accuracy and the T^{-2} coefficient for each proton contains crucial information on J and D parameters. Nevertheless, in the case of the series of dinuclear high-spin nickel(II) studied, deviations to the strict Curie law are too small on the temperature range studied to determine precisely either the nature (J and/or D) or the exact value of these parameters (it can only be estimated to be on the order of a few cm^{-1} on the basis of a b'/a' analysis from Table 3). This observation is in complete agreement with the plateau observed from magnetic susceptibility data $\chi T = f(T)$ between 188 and 298 K (see Supporting Information). Similar behavior and results are obtained for **b(PF$_6$)$_2$** and **c-(PF$_6$)$_2$**, as reported in the Supporting Information.

Relaxation Properties in a(BPh$_4$)$_2$. This dimer presents a small ferromagnetic coupling constant ($J = 2.5$ cm^{-1}) as emphasized through SQUID measurements and NMR temperature-dependence studies. Relaxation rates, T_1^{-1}, can consequently be handled in the point dipole approximation[20,22] and are expected[55,56] to be proportional to the sum $r_{Ni1\cdots H}^{-6} + r_{Ni2\cdots H}^{-6}$, where Ni_1 is the closest metal atom to the considered proton H. Crystal structure data and Thio-*H3* longitudinal relaxation time are used in this calculation. Results are reported

(52) Reference 11, pp 52−55.

(53) Kurland, R. J.; McGarvey, B. R. *J. Magn. Reson.* **1970**, *2*, 286−301.

(54) Shokhirev, N. V.; Walker, F. A. *J. Phys. Chem.* **1995**, *99*, 17795−17804.

(55) Banci, L.; Bertini, I.; Luchinat, C. In *Nuclear and electron relaxation*; VCH Publishers: New York, 1991; pp 91−122 and 143−162.

(56) If the correlation time in a homodimer is considered to be the same for each spin-level, T_1^{-1} in the coupled system is equal to half that in the uncoupled system (see ref 53).

Table 3. Temperature Dependence of Chemical Shifts and Relaxation Rates for **a(BPh$_4$)$_2$** in CD_2Cl_2

resonance assignment		δ (ppm)[a]	Curie plot[b] δ_{int} (ppm)[b]	Curie plot[b] $a \times 10^{-3}$ [b] (ppm·K)	polynomial plot[c] δ_{dia} (ppm)[c]	polynomial plot[c] $a' \times 10^{-3}$ [c] (ppm·K)	polynomial plot[c] $b' \times 10^{-5}$ [c] (ppm·K^2)	T_1^{-1} sloped[d] $\alpha \times 10^{-3}$ [d] (ms^{-1}·K^2) (*R*)
Py1+2	H1	155.03	−2.85	44.7	8.49	45.5	6.4	*h*
		171.78	−0.23	50.3	8.49	41.8	3.6	*h*
Py1	H2	52.04	5.85	13.5	7.29	12.8	0.8	26.1(0.991)
	H3	16.30	6.85	2.8	7.29	2.6	0.2	10.6(0.982)
	H4	51.20	4.86	13.6	7.60	12.2	1.6	28.7(0.987)
Py2	H2	48.38	5.51	12.5	7.29	11.7	1.0	26.1(0.996)
	H3	14.15	6.14	2.3	7.29	1.8	0.6	10.1(0.976)
	H4	48.38	5.51	12.5	7.60	11.6	1.2	26.1(0.996)
Thio	H1	∼ 5.32[e]	7.09	−0.5	7.35	−0.6	0.2	*e*
	H2	15.33	6.86	2.5	7.35	2.2	0.2	7.9(0.988)
	H3	0.09[e]	7.88	−2.3	7.35	−2.0	−0.3	*e*
	H4	12.36	6.86	1.6	7.35	1.4	0.2	20.8(0.981)
CH_2 H_{eq}	Py *trans*[g]	137.80	−6.53	42.2	3.80	37.3	5.8	*h*
	Py *cis*[g]	245.82	−3.54	75.5	3.80	70.0	11.0	*h*
	Thio	112.28	−18.64	38.3	3.86	27.5	12.6	*h*
CH_2 H_{ax}	Py *trans*[g]	∼7.5[f]	17.53	−5.1	3.80	−7.1	1.1	*e*
	Py *cis*[g]	0.09[e]	2.50	16.5	3.86	15.6	1.2	*h*
	Thio	59.29						
OAc	CH_3	25.99	2.16	7.0	2.50	6.2	0.9	26.1(0.991)

[a] Observed chemical shifts, in ppm, at 293 K. [b] Fit of the chemical shift variations (in ppm) with temperature (in K), according to the Curie law: $\delta_{obs} = \delta_{int} + a/T$, where δ_{int} is the intercept at infinite temperature and a is the Curie slope. The correlation coefficient is greater than 0.99 in each single case. [c] Fit of the chemical shift variations (in ppm) with temperature (in K), according to a polynomial function: $\delta_{obs} = \delta_{dia} + a'/T + b'/T^2$, where δ_{dia} is the observed diamagnetic shift in the free ligand. The correlation coefficient is greater than 0.99 in each single case. They do not significantly differ from the values obtained in the case of the Curie law. [d] Fit of the relaxation rate T_1^{-1} (ms^{-1}) with the temperature (in K), according to the following expression: $T_1^{-1} = \alpha/T^2$. The correlation coefficients are given within parentheses. T_1 values of CH_2 H_{ax} and CH_2 H_{eq} are very difficult to follow with temperature, as relaxation times get lower with temperature. Fitting results are not given due to the small number of available data. [e] Fortuitous overlap at 293 K, which can be solved through temperature change. [f] Resonance buried under the BPh_4^- peak. [g] Methylene group bound to the pyridyl ring fixed to the metal in a trans (respectively cis) configuration with respect to the thiophenolic group. [h] T_1 values are too short when temperature is decreased. Low reproducibility of T_1 measurement forbid curve fitting.

in Table 2, which shows good agreement with experimental T_1 values, especially for methylene protons. In the case of aromatic ring protons, increased differences are observed, which can arise from slight discrepancies between the solid-state and solution structures of the dinuclear complex (especially ring flipping) or from electron spin-delocalization and contact interactions within the ring. Nevertheless, qualitative agreement is substantial within a specified aromatic ring and thus confirms, if needed, proposed assignments. It can be noted that distinction of the two pyridyl rings (cis or trans with respect to the thiophenolic anchor on the nickel atom) remains hazardous, due to high similarity of measured T_1 values for protons occupying equivalent positions on the two different rings and despite clear distinct parameters in the solid state. These results are indications in favor of pyridyl rings flipping around an equilibrium position in solution.

Whether temperature is also a relevant factor is addressed next. Decreasing the temperature of a **a(BPh$_4$)$_2$** solution in dichloromethane induces an increase in the longitudinal relaxation rates. This observation can only be explained if electronic spin-relaxation overcomes all relaxation mechanisms and if the nuclear spins interact with a time-averaged electron magnetic moment. This rather unusual behavior is quantitatively reproduced in Figure 8 in the particular case of Py1-*H2* for $188 \leq T$ (K) ≤ 298. Least-squares fit procedures are carried out using alternatively linear or second-order polynomial regression. A mathematically and physically acceptable result is obtained for a T^{-2} fit of the relaxation rate T_1^{-1} (correlation coefficient = 0.991 and slope = 26081 ± 180 K^2·ms^{-1}). When applied to **a(BPh$_4$)$_2$** protons for which the number of T_1 data are numerous enough, this procedure gives the results reported in Table 3. Interestingly, the slope of detected relaxation rate vs the square of the inverse temperature is related to the distance between the proton of interest and the nickel centers, and it is highly consistent with what has been shown for calculated T_1 values

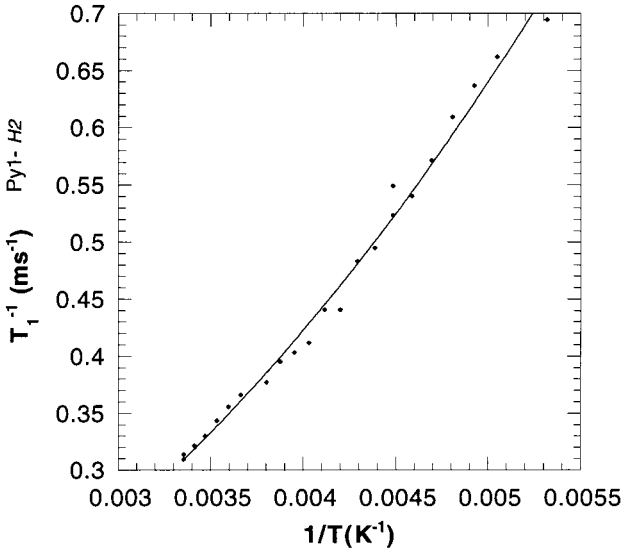

Figure 8. Observed relaxation rate vs reciprocal temperature for the resonance assigned to Py1-*H2* for **a(BPh$_4$)$_2$** in CD_2Cl_2. The result of a second-order polynomial least-squares fit, $T_1^{-1}(ms^{-1}) = a + b/T + c/T^2$ (T in K), is shown with the solid line: $a = 0.06$ ms^{-1}, $b = -10$ K·ms^{-1}, $c = 2.5 \times 10^{-3}$ K^2·ms^{-1}, and correlation coefficient = 0.995.

at 293 K. These data are then strong evidence in favor of a dominant Curie longitudinal relaxation mechanism, where, according to Clementi and Luchinat:[57]

$$T_1^{-1} = \frac{2}{5}\left(\frac{\mu_0}{4\pi}\right)^2 \frac{\gamma_n^2 g_e^2 \mu_B^2}{r^6 (3k_B T)^2}\left[f(J,D)\frac{3\tau_c}{1+\omega_n^2\tau_c^2}\right] \qquad (4)$$

f(J,D) being almost temperature independent when J, $D \ll k_B T$ and $\tau_c^{-1} = \tau_r^{-1} + \tau_m^{-1}$. If Curie behavior has been supported

by experimental data in the case of transverse relaxation, complex **a(BPh$_4$)$_2$** is, to our knowledge, the first example of this type for longitudinal relaxation. This pattern is nevertheless common to the whole series of high-spin nickel(II) dimers, as **b(PF$_6$)$_2$** and **c(PF$_6$)$_2$** present the same characteristics (see Supporting Information).

NMR and Magnetic Properties of High-Spin Nickel(II) Complexes. Despite extremely short longitudinal relaxation times (the longer T_1 for **a(BPh$_4$)$_2$** is 11.41 ms at 293 K), resonances in dinuclear high-spin nickel(II) complexes have all been identified. This results from a combination of 2D NMR, specific site-directed chemical substitution, as well as relaxation and chemical shift temperature dependence data. Comparison of calculated and experimental T_1 values shows that solid-state structure persists in solution and allows the dipolar relaxation mechanism to be established as a major pathway. The assignment strategy developed here for **a(BPh$_4$)$_2$** applies successfully in the case of **b(PF$_6$)$_2$** and **c(PF$_6$)$_2$** and is most probably general to every dimeric species containing two weakly ferromagnetically coupled high-spin nickel(II)s.

The same strategy nevertheless appears to remain hopeless in the case of high-spin nickel(II) monomers. This is due to intrinsic line widths, which are about 1 order of magnitude sharper in the dinuclear nickel(II) complexes than in the equivalent monomer. An analogous situation has been described for dinuclear vs mononuclear copper(II) complexes, independently of the sign and size of the magnetic coupling between the two metal centers.[20,22] In the case of weakly coupled dinuclear copper(II) complexes, where relaxation mechanisms are dominated by dipolar contribution,[22] the sharpness of NMR signals is due to shorter electronic relaxation times in dimeric vs monomeric species. Among other factors, the proximity of the two metal ions, flexibility around them due to ligand structure, and electronic delocalization are suggested to be responsible for this observation. Modulation of zero-field splitting of the total spin-state $S' = 1$ in the coupled systems is considered, according to the authors,[22] a likely source of electron-relaxation. In the case of homodimers containing high-spin nickel(II) in a mixed N/O/S environment, the present study shows that the predominant longitudinal relaxation mechanism occurs via a Curie dipolar mechanism. T_2 relaxation times in the dimer show similar behavior with temperature as T_1, i.e., increasing transversal relaxation rates with decreasing temperature, thus suggesting an analogous relaxation mechanism. The electron contribution to nuclear relaxation is then given by the interaction between the time-averaged electron magnetic moment and the nucleus. Amazingly, experimental T_1 values do not significantly differ for high-spin nickel(II) complexes, when going from the dimer to the monomer. On the other hand, transversal relaxation rates are 1 order of magnitude longer in the monomer **m(BPh$_4$)** than in the dimer **a(BPh$_4$)$_2$**. These results suggest then different contributions to T_2 relaxation pathways in the dimer vs the monomer. The possibility that the signals are narrower in the dimer due to magnetic coupling is unlikely, because the small ferromagnetic coupling allows all spin-states to be largely populated in the temperature range of interest. Implications of intrinsic zero-field splitting, arising independently from each nickel atom, and overall $S' = 2$, 1, or 0 zero-field splitting can be considered next. Magnetic anisotropy in the dimer, which presents a pseudo-C_2 axis, is expected to differ from the anisotropy in the corresponding monomer that contains a distorted octahedral nickel atom. A stronger zero-field splitting in the monomer would then render enhanced transversal relaxation rates and would be consistent with the observations.

Relaxation times in the present series of high-spin nickel(II) dimers are sensitive to the counterion nature. Replacement of the electronrich BPh_4^- by the smaller PF_6^- anion in **a(BPh$_4$)$_2$** induces an overall relaxation time lengthening of the corresponding protons by a factor of 1.1 to 1.6, in dichloromethane solution (T_1 values are provided in the Supporting Information). When Py-*H1* protons are substituted by methyl groups such as in the case of **b(PF$_6$)$_2$**, comparison of the T_1 data also shows a uniform decrease in the observed relaxation rates (T_1 values given in the Supporting Information). On the other hand, when the behavior of the observed chemical shifts vs inverse temperature is compared for **a(BPh$_4$)$_2$** and **b(PF$_6$)$_2$**, the T^{-1} and T^{-2} slopes are similar in the two complexes. The *J*-coupling constant value, which is mainly dependent on the bridges geometry, is not expected to be highly modified through pyridyl chemical substitution. On the contrary, fluctuations in geometry around the nickel atom and intermolecular interactions may affect the zero-field splitting of each individual nickel atom and consequently the zero-field splitting of the total $S' = 2$ and 1 spin-states. The observations are then consistent with a dominant *J*-dependence on chemical shift and a dominant *D*-dependence on relaxation times in the nickel(II) dimers. This emphasizes the possible role of zero-field splitting magnitude in the detection of sharper resonances in the case of dimers vs monomers. Both parameters are nevertheless in the case of the studied dimers very small and these proposed explanations must be applied to a larger number of dinuclear high-spin nickel(II) complexes.

Conclusion

The aim of controlling the preparation of six-coordinated nickel(II) amine−thioether complexes has been achieved by using the cyanoethyl-protected thiolate in the N_3SR ligand series. Reaction with $Ni(OAc)_2 \cdot 4H_2O$ in alcohol allows the simple and controlled preparation of both mono- and dinuclear nickel(II) complexes. This synthetic strategy has provided a well-characterized μ-disulfide dinuclear Ni^{II} complex **a(BPh$_4$)$_2$**. A second complex **m(BPh$_4$)** has been isolated from the dinuclear complex synthesis and spectroscopically characterized as a mononuclear Ni^{II} octahedral complex. Our data demonstrate, for the first time, that ^{1}H NMR spectra can be easily obtained for weakly ferromagnetically spin-coupled dinuclear octahedral Ni^{II} centers. In this particular case, despite very short relaxation times, a complete assignment strategy has been performed. This allowed further establishment of the main relaxation pathways through temperature-dependence studies. Analysis of chemical shift behavior vs temperature demonstrated the occurrence of the weak spin−spin coupling constant and/or zero-field splitting in these complexes. The precise determination of these parameters is hazardous in this case, due to the relative insensitivity of magnetic susceptibility in the accessible temperature range. Nevertheless, the established procedure, as well as the NMR feasibility, would then open large perspectives for the study of an increasing number of high-spin nickel(II) dimers. Applying it to strongly antiferromagnetically coupled systems would provide essential data, to get further insight into understanding the relaxation mechanisms in dimers and to compare it to the one in monomers. From the structural point of view, these results also suggest that ^{1}H NMR in Ni^{II} high-spin species may be used for wild-type or engineered dinuclear nickel metalloproteins to probe the local coordination environment around the metallic center.

(57) Clementi, V.; Luchinat, C. *Acc. Chem. Res.* **1998**, *31*, 351−361.

Acknowledgment. The authors are grateful to Dr. Stéphane Ménage and Dr. Serge Gambarelli for their interest in this work and fruitful discussions.

Supporting Information Available: Experimental details relative to the syntheses of **6**, **7**, and **9** and detailed characterization of compounds **1** to **4** and **6** to **9**; syntheses and physicochemical properties of the complexes **a(PF$_6$)$_2$**, **b(PF$_6$)$_2$**, **c(PF$_6$)$_2$**, and **m(PF$_6$)**; crystallographic experimental details for **a(BPh$_4$)$_2$** (Table 1S) and an ORTEP plot showing the entity **a$_2$** from complex **a(BPh$_4$)$_2$** (Figure 1S); magnetic susceptibility data $\chi T = f(T)$ for **a(BPh$_4$)$_2$** (Figure 2S); ^{1}H COSY spectrum of **b(PF$_6$)$_2$** and **c(PF$_6$)$_2$** (Figures 3S and 4S); resonance assignment, relaxation properties, and dependence in temperature of **a(PF$_6$)$_2$**, **b(PF$_6$)$_2$** (Table 2S), and **c(PF$_6$)$_2$** (Table 3S); Curie law deviations due to *D* and *J*; and linear least-squares fit of experimental relaxation rate vs reciprocal temperature of Py1-*H2* resonance for **a(BPh$_4$)$_2$** in CD_2Cl_2 (PDF). An X-ray crystallographic file for **a(BPh$_4$)$_2$** (CIF). This material is available free of charge via the Internet at http://pubs.acs.org.

JA010342K